Arcyriaflavin A as a Potential Therapeutic Agent for Osteoporosis

Doctoral Thesis

to obtain a doctorate (Dr. med.)

from the Faculty of Medicine

of the University of Bonn

Mengbo Zhu

from Shanxi China 2025

Written with authorization of the Faculty of Medicine of the University of Bonn
First reviewer: UnivProf. Dr. rer. nat. Frank A. Schildberg Second reviewer: PD Dr. Stilla Frede
Day of oral examination: 11.09.2025
From the Department of Orthopedics and Trauma Surgery / University Hospital Bonn

Table of contents

List of abbreviations	5
1. English summary	7
1.1 Introduction	7
1.2 Method and Material	10
1.2.1 Cell Culture	10
1.2.2 Medium composition	12
1.2.3 Arcyriaflavin A preparation and biosafety	13
1.2.4 Phenotype Assay	14
1.2.5 Function Assay	16
1.2.6 Molecular analysis	18
1.2.7 Efficacy test in human cells	23
1.2.8 Ovariectomy Mouse Model	24
1.2.9 Statistical Analysis	25
1.3 Results	26
1.3.1 Biosafety assay	26
1.3.2 Morphology analyses	26
1.3.2.1 TRAP staining	26
1.3.2.2 Fluorescence staining	27
1.3.3 Molecular analyses	29
1.3.3.1 PCR	29
1.3.3.2 Western Blot	30
1.3.3.3 Early-stage signaling pathway	30
1.3.4 Resorption assay	31
1.3.5 Animal experiments	32
1.3.6 Human cells	33
1.4 Discussion	34
1.5 Summary	42
1 6 References	43

2. Publication	53
3. Declaration of Personal Contribution	54
4. Acknowledgement	56

List of abbreviations

ArcyA Arcyriaflavin A

APS Ammonium persulfate

BMMs Bone marrow derived macrophages

BRC bone remodeling compartment

BSA Bovines' serum albumin

BV/TV Bone volume/Total volume

CCK8 Cell Counting Kit-8

ETC Electron transport chain

cDNA Complementary deoxyribonucleic acid

DMSO Dimethyl sulfoxide

DPBS Dulbecco's phosphate-buffered saline

EDTA Ethylenediaminetetraacetic acid

F-actin Filamentous actin

GAPDH Glyceraldehyde-3-Phosphate Dehydrogenase

HCL Hydrogen chloride

HSCs Hematopoietic stem cells

HEPES 4-(2-hydroxyethyl)-1-piperazine ethane sulfonic acid

M-CSF Macrophage colony-stimulating factor

α-MEM alpha-Minimum Essential Medium

MNCs Multiple nuclei cells

OBs Osteoblasts

OCs Osteoclasts

OD Optical density

OF Osteoporotic fractures

ONFH Osteonecrosis of the femoral head

OP Osteoporosis

OPG Osteoprotegerin

OVX Ovariectomy

P/S Penicillin/Streptomycin

PBMCs Peripheral blood mononuclear cells

PBS Phosphate-buffered saline

PCR Polymerase chain reaction

RANKL Receptor activator of nuclear factor kappa-B ligand

RIPA buffer Radioimmunoprecipitation assay buffer

RNA Ribonucleic Acid

ROI Regions of interest

SEM Scanning Electron Microscope

TBS Tris-buffered saline

TBST Tris-buffered saline with Tween® 20

TEMED Tetramethyl ethylenediamine

TRAP Tartrate resistant acid phosphatase

1. English summary

1.1 Introduction

The ageing of the global population is a central theme in healthcare practice and research during the first half of the 21st century. According to WHO survey data, the elderly population is projected to surge from 2000 to 2050. Especially, the numbers of individuals older than 60 and 80 are expected to double and triple respectively (Bautmans et al., 2022). Meanwhile, the low birth rate, along with staff shortage and insufficient treatment capacity, is loading increasing burden on overwhelmed healthcare system. Taking nursing as an example, there were 590,000 vacancies in European nursing in 2020, and this gap continues to widen (Tamata et al., 2023). According to epidemiological studies, inindividuals over 50 are at high risk for osteoporosis (OP), with the incidence being twice as high in women as in men. Postmenopausal women are high-risk population but not alone. In addition to estrogen withdrawal and ageing, factors such as inappropriate use of steroids, insufficient intake of calcium and vitamin-D, smoking, and alcohol abuse contribute to the development of OP (Lane 2006, Le Dare et al., 2019).

Unlike other aging-related diseases, OP is often overlooked because its primary symptom, bone mass loss, is not immediately noticeable. However, the complications of OP can be severe, even life-threatening. Fractures associated with OP are particularly concerning, as they frequently result in serious clinical consequences. Clinical data demonstrated that the frequently-occurring sites are forearms, hip, and vertebrae (Clynes et al., 2020). Notably, hip fracture, usually resulting from fall from standing, is associated with high morbidity, nearly 100 % hospitalization, and most post-fracture complications such as pressure sores, bronchopneumonia, and osteonecrosis of the femoral head (ONFH) (Assouline-Dayan et al., 2002, European Prospective Osteoporosis

Study et al., 2002). Moreover, OP is closely linked to cervical spondylosis, lumbar vertebrae disease, arthritis, and pain (Alsoof et al., 2022, Funck-Brentano et al., 2011, Oleksik et al., 2000).

According to a survey on the proportion of medical expenditure by various diseases in the United States between from 2000 to 2011, the in-hospital cost due to osteoporotic fractures (OF) was approximately 5.1 billion per year, surpassing that of myocardial infarction and stroke. The highest cost of OF was attributed to the large number of hospitalizations which was 4.9 million cases in total (Singer et al., 2015). An estimate in 2010 predicted that the medical cost incurred by osteoporotic hip fracture alone would excess \$130 billion by 2050 (Harvey et al., 2010). Regrading Europe, a European guidance for osteoporosis reported that the disease accounted for a direct cost of 38.7 billion in 27 EU countries over the past decade. The guideline also noted that the most fatal complications of OP are hip and spine fractures, which account for 50 % and 28 % of the osteoporosis-related deaths, respectively (Kanis et al., 2013). Beyond the measurable expenditure, the potential costs in other areas are too numerous to count.

The complexity of OP in terms of etiology and diagnosis is related to its multifaceted cellular and molecular mechanisms. In essence, the pathological causes of OP can be concluded as an imbalance in bone remodeling, including inadequate osteogenesis or exceeded bone resorption. Throughout life, bone remodeling is a continuous process mediated by two distinct cell types: osteoclasts (OCs), which resorb obsolete bone, and osteoblasts (OBs), which form new bone through mineralization. When the bone remodeling is out of this delicate dynamic balance, OP develops. Among these processes, excessive bone resorption by OCs plays a dominant role in the development of imbalances (Andersen et al., 2009, Katsimbri 2017, Kim et al., 2020).

Based on the understanding of the pathological mechanism of OP, OC has been identified as a crucial target for prevention and alleviation of osteoporosis. Numerous therapies have been developed to inhibit OC differentiation and function, including denosumab, bisphosphonates, parathyroid hormone analogues, and estrogen-related therapy (LeBoff et al., 2022, Reid et al., 2022). However, these therapies are not without limitations. For instance, denosumab, a targeted therapy, is associated with a significant rebound effect, leading to multiple spontaneous vertebral fractures upon discontinuation. The current solution is consolidative bisphosphonate treatment after denosumab dose. Nevertheless, an exact and effective strategy for consolidative therapy remains elusive (Lamy et al., 2019). Bisphosphonates, which are the same first-line therapies like denosumab, are not perfect. In addition to causing stress on digestive and metabolic organs (stomach, liver, and kidneys), long-term bisphosphonate use increases the risk of atypical subtrochanteric and diaphyseal femoral fractures, as well as osteonecrosis of the jaw (Khan et al., 2015, Shane et al., 2014). The conception of "drug holiday" has been introduced to minimize potential side-effects of continuous bisphosphonate treatment. However, current clinical algorithms are not consistent due to different daily habits and customs of individuals (Lee et al., 2015, Li et al., 2013).

Therefore, in our study we sought to propose a novel potential solution from a different perspective. Previous studies have reported that M2 macrophages serve as a negative regulator of OCs differentiation and function, whereas M1 macrophages are the precursors of OCs, in addition to secreting pro-osteoclastogenic cytokines (Hu et al., 2023, Kim et al., 2009, Munoz et al., 2020, Souza et al., 2013). We identified an underexplored compound, Arcyriaflavin A (ArcyA), which has been reported to promote M2 polarization (Hu et al., 2021). Building on this, we evaluated ArcyA's cytotoxicity and bio-safety, and further investigated its potential effects on osteoclastogenesis in both *in vitro* and *in vivo*. Our findings demonstrated, for the first time, that ArcyA inhibited OC

differentiation and function *in vitro*, and ameliorated estrogen deprivation-induced OP in mouse models.

1.2 Method and Material

1.2.1 Cell Culture

The study primarily focused on osteoclasts. Hence the induction of OCs from bone marrow derived macrophages (BMMs) was the cornerstone.

In the laboratory setting, the RAW 264.7 cell line and primary cells are both commonly used for OC differentiation. In this study, primary cells were used because they more closely resemble the *in vivo* situation, compared to a cell line that underwent multiple passages.

Following euthanasia, tibiae and femora were harvested from 6-week-old C57BL/6 mice (Charles River Laboratories Germany). During dissection, contamination with other tissues (hair, skin, fat tissue, and muscle) ought to be carefully avoided.

Contaminants from hair and skin could introduce external pollutants into the culture system; while fibroblast from muscle tissue might interfere with differentiation and migration of OC precursors.

To extract bone marrow, the bone marrow cavity was fully exposed. A 1-mL syringe was used to flush out the bone marrow from tibia and femora. To avoid cell damage, repetitive aspiration was minimized. 1 mL pipette tips (Eppendorf Vertrieb Deutschland GmbH, Germany) were employed for cell resuspension.

The resuspended bone marrow was cultured in a 100 x 22mm tissue culture

dish (Th. Geyer, Germany, Art-Nr: 7696774) with 10mL of M-CSF+αMEN medium (details of the medium composition are provided later) for 24 hours. During the first 24 hours, BMMs adhered the bottom of the plate, while non-adherent cells (e.g., red blood cells and platelets) were removed during a medium change. It is crucial to replace the medium and wash with dulbecco's phosphate-buffered saline (DPBS, Gibco, Thermo Fisher MA, USA, REF:14190-094) gently as the adherence of BMMs at this stage is not tight.

Usually, the maturation of BMMs typically requires 4-5days. Mature BMMs appear mostly polygonal, with rare pseudopodia, and are half-adherent (This is very similar to RAW264.7 cells). Trypsin-Ethylenediaminetetraacetic acid (Trypsin-EDTA, Gibco, REF: 15400-054) is commonly used for passage and seeding of BMMs, but not for detachment. A short trypsinization (1-2 minutes) prevents cell damage caused by shear force during pipetting.

Depending on experimental purposes, BMMs can be seeded into different plates at various cell densities. After 24 hours for adherence and adaptation, the macrophage colony-stimulating factor (M-CSF) + α MEN was replaced by receptor activator of nuclear factor kappa-B ligand (RANKL) + α MEM medium, marking this time point as day0.

Under the induction of RANKL, BMMs differentiated to OCs over 5-6 days. By day1, some cells became round. From day3 to day5, cell fusion occurred, and multinuclear cells began to form and mature (Figure 1).

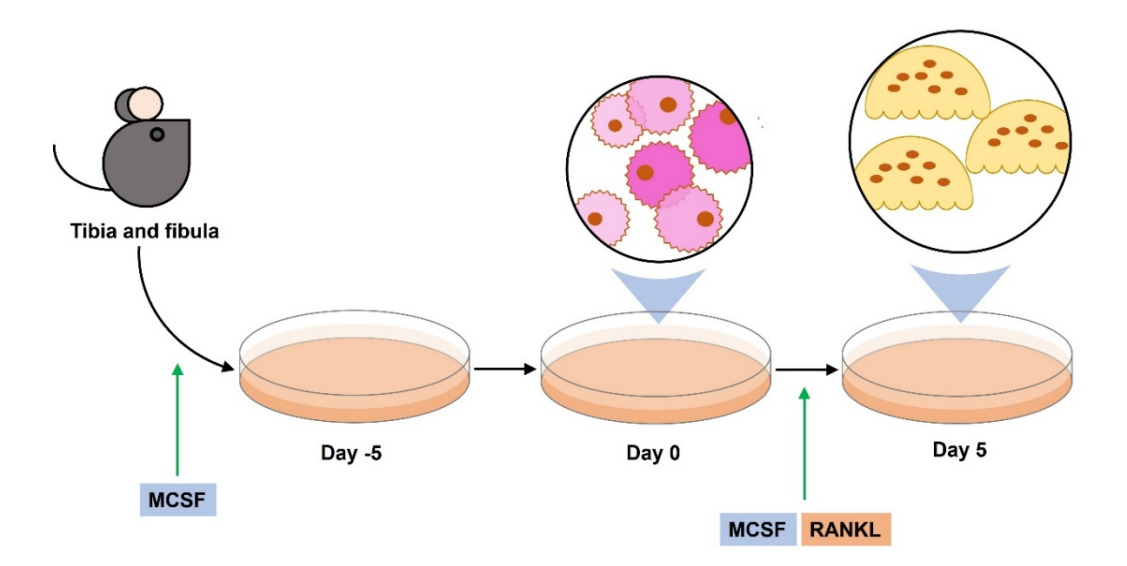


Figure1: The osteoclast differentiation procedure. M-CSF is essential for macrophages differentiating from myeloid progenitors. Therefore, the presence of M-CSF in the early phase is necessary for the sufficiency of mature BMMs at day0. Insufficient BMMs lead to lack of OC precursors and further failure of multinuclear cell formation. The image is drawn using Microsoft Office PowerPoint.

1.2.2 Medium composition

BMM induction medium was prepared using complex alpha-Minimum Essential Medium (α-MEM) medium adding mouse M-CSF (Miltenyi Biotec, Germany, Nr. 130-094-129) at a concentration of 50ng/mL. To prepare OCs induction medium, RANKL (Miltenyi Biotec, Nr. 130-094-646) at a concentration of 50ng/mL was added to the BMM induction medium.

Complex α -MEM was prepared by supplementing Alpha minimum essential medium (α -MEM, Gibco, REF: 22571-020) with the following components: Penicillin-Streptomycin (P/S, Gibco, REF: 15140-122) preventing potential contamination, HEPES (Carl Roth, Germany, Art-Nr: HN78.2) for pH stabilization, fetal bovine serum of U.S. origin (Gibco, REF: 26140-079) and L-Glutamine 200mM (Gibco, REF: 25030-024) providing essential nutrients for cell growth.

The ratio is 10mL Penicillin-Streptomycin, 1g 4-(2-hydroxyethyl)-1-piperazine

ethanesulfonic acid (HEPES), 10mL L-Glutamine, 50mL serum for every 500mL α-MEM.

Notably, L-Glutamine is critical for proliferation of actively dividing cells but is unstable in solution. Therefore, the medium containing L-Glutamine should be used promptly after preparation.

For a clearer expression of the media composition, the formulas of medias for various experimental purposes are listed below:

M-CSF medium	RANKL medium
α-MEM 500mL	α-MEM 500mL
Penicillin/Streptomycin (P/S) 10mL	P/S 10mL
Fetal bovine serum 50mL	Fetal bovine serum 50mL
L-Glutamine 10mL	L-Glutamine 10mL
HEPES 1g	HEPES 1g
M-CSF 50ng/mL	M-CSF 50ng/mL + RANKL 50ng/mL

1.2.3 Arcyriaflavin A preparation and biosafety

Arcyriaflavin A (ArcyA) was obtained from Santa Cruz Biotechnology (TX, USA, CAT:sc-202470, CAS No:118458-54-1). For long-term storage, ArcyA was kept in dry powder form at -80°C. For routine use, ArcyA was dissolved in Dimethyl sulfoxide (DMSO) at a concentration of 10mM in -20°C for accessibility. DMSO was produced by AppliChem GmbH (Germany, Nr. A3672). Based on different experimental requirements, the stock solution can be further diluted to achieve the wanted working concentrations.

WST-8 (2-[2methoxy-4-nitrophenyl]-3-[4-nitrophenyl]-5-[2,4-Disulfophenyl] - 2H-tetrazolium) solution (Cell Counting Kit-8, Dojindo Laboratories, Japan, Code No. CK04) provides a simple and rapid method for accurately assessing cell viability. BMMs were seeded in 96-well plates (Greiner, Austria, Cat-No.655180) at a density of 1x10^4 cells per well and divided into 4 groups,

including one control group (5 wells per group). The BMMs were firstly cultured in M-CSF medium for 24h adaption and then treated with ArcyA at various concentrations (0µmol/mL [DMSO only], 1µmol/mL, 2.5µmol/mL, and 5µmol/mL). The cells were cultured under the presence or absence of ArcyA for 5 days with medium changes every two days. On day 5, 10µL WST-8 solution was added to each well and incubated at 37°C for 4 hours. A separate row of wells without cells, containing 100µL medium with ArcyA at concentrations matching the experimental groups, were included as blank control to account for potential interference from ArcyA. The absorbance of 450nm, reflecting cell viability, was measured by the SPARK® Microplate reader (Tecan Deutschland Gmbh, Germany).

1.2.4 Phenotype Assay

The number of tartrate resistant acid phosphatase (TRAP) positive cells and OC area are commonly used microscopy parameters to evaluate the activity of OC differentiation.

We employed the same cell seeding strategy for both TRAP and florescence staining: BMMs were seeded in 96-well plates at a density of 1x10⁴ cells per well. During the first 24h after seeding, the cells were cultured with M-CSF medium for adaption. Following the adaption period, M-CSF medium was replaced by medium with different supplements corresponding to grouping strategy.

The grouping was as following:

	NC	PC	1µmol/ml	5µmol/ml
M-CSF	50ng/ml	50ng/ml	50ng/ml	50ng/ml
RANKL	/	50ng/ml	50ng/ml	50ng/ml
Arcyriafiavin A	1	1	1µmol/ml	5µmol/ml

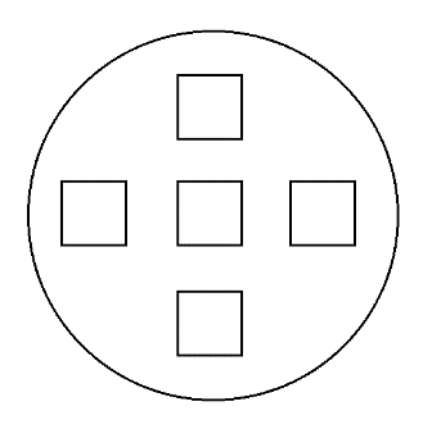
(NC represents Negative control; PC represents Positive control)

BMMs were cultured with in respective medium for 5 days, with medium

changes every 2 days. By day 5, the culture was terminated, and cells were fixed with 4 % formalin (Roti®Histofix, Carl Roth, Germany, Art.-Nr. P087.5) for TRAP staining, or 4 % Paraformaldehyde (MORPHISTO GmbH, Germany, REF: 11762.01000) for fluorescent staining. Different fixation reagents were chosen based on their specific advantages: formalin ensures stronger adherence to the bottom, and reduces potential exfoliation TRAP staining; while paraformaldehyde preserves protein structures and benefits the combination between fluorescent dye and binding sites.

Cells fixed for TRAP staining were washed with DPBS for 3 times and pretreated with TRAP buffer (formula described later) at room temperature for 10min. TRAP dye solution (formula described later) was then added into wells and incubated at 37°C for approximately 1 hour. The reaction could be terminated slightly earlier or later to avoid insufficient or excessive staining.

The stained cells were covered with DPBS and imaged under a bright field microscope for further quantitative analysis. Five predefined 0.01mm² sampling regions were selected as shown in the accompanying figure. TRAP positive cells in each region were manually counted.



All red stained cells with more than 3 nuclei were identified as TRAP positive cells. Due to the uneven distribution of multinuclear cells, sampling regions should be selected from both the central and peripheral areas in each well. Furthermore, the absolute number of TRAP positive cells was recorded instead of calculating relative ratios.

Formula of TRAP buffer and TRAP dye solution are listed below

TRAP buffer	TRAP dye solution	
 ※1.64g Sodium Acetate (AppliChem GmbH, Nr. 131633) ※ 5.75g Sodium tartrate dihydrate (Carl Roth, ArtNr. T110.2). ※H2O adjusted to 250mL ※pH 5.0 	※1mg Naphthol AS-Mix Phosphate (AppliChem GmbH, REF: N5000) ※ 100μL N-N-Dimethylformamide (Sigma-Aldrich, REF: 319937) ※ 6mg Fast Red Violet LB Salt (Sigma-Aldrich, REF: F3381) ※10mL TRAP Buffer	

The cells designated for fluorescent staining were pretreated with 0.1 % Triton X-100 (Sigma-Aldrich, MA, USA, REF: 319937 and REF:X100) to enhance membrane permeability. Phalloidin-iFluor 647 and DAPI (4',6-diamidino-2-phenylindole, Abcam, British, REF: ab176759 and ab285390) were used to stain cytoskeleton and nucleus after 30min (BSA, Carl Roth, Germany, Art.-Nr. 0163.2) blockade with bovine serum for preventing non-specific binding. Phalloidin-iFluor 647, a specific probe for filamentous actin (F-actin), emitted red fluorescent; while DAPI, a nuclear specific stain, emitted blue fluorescent.

All microscopy was performed with an Olympus IX81 microscope equipped with a DP80 microphotographic camera (Olympus, Japan).

1.2.5 Function Assay

To assess the resorption function of OCs, we applied advanced bonelike apatitic calcium phosphate coating layer technology, which offers several advantages over the commonly used bone-cutting slides assay. Based on a protocol by Tas and Bhaduri, an apatitic calcium phosphate layer was coated onto 96-well plates at a thickness of 20-65µm and a relatively high bonding strength (12±2 MPa). The OCs resorbed the coating layer and generated resorption pits exposing transparent plastic well bottom of the wells. The remaining non-resorbed coating layer was stained black using silver nitrate (Carl Roth, Art-Nr: 9370.4).

In contrast to bone-cutting slides, which are harvested from bovine bone with limited standardization and the requirement of SEM (Scanning Electron Microscope) to visualize resorption pits, the bonelike apatitic calcium phosphate coating plates reduce assay time while offering a higher successful rate.

The same grouping and culturing strategy used in the phenotype assay was applied here. BMMs, divided into 4 groups, were seeded into coated 96-well plates at a density of 1x10^4 cells per well. The assay was terminated on day 5. To fully expose the resorption pits, cells were removed using 5 % Sodium thiosulfate (formula described later). Subsequentially, the Sodium thiosulfate solution was replaced with 5 % silver nitrate solution (formula described later) and incubated in the dark for 30min, allowing sliver to precipitate and deposit onto residual coating layer. Finally, sodium carbonate-formaldehyde solution (formula described later) was used to fix the dye via a neutralizing reaction. Pure ethanol was then employed to cover and preserve staining results for long-term storage.

Formulas of reagents abovementioned are listed:

5 % Sodium	5g Na ₂ S ₂ O3 (Carl Roth, Art-Nr: HN25.1)
thiosulfate	adjusting to 100mL by H ₂ O
5 % Silver nitrate	5g silver nitrate (Carl Roth, Art-Nr: 9370.4)
solution	adjusting to 100mL by H ₂ O
	5g Na ₂ CO ₃ (Carl Roth, Art-Nr: A135.1)
Sodium carbonate-	25mL 37 % Iger formaldehyde solution (Labomedic,
formaldehyde	Germany, Art-Nr: 2142694)
solution	adjusting to 100mL by H ₂ O
1	

Under a bright field microscope, the stained coating appeared black, while the transparent resorption pits were white. By selecting appropriate threshold,

ImageJ software (Ver.1.46r) was used for quantifying the resorption pit area.

1.2.6 Molecular analysis

We seeded BMMs in 6-well plates at a density of 3.0x10⁵ per well for 5days (medium changing every 2 days). Cells designated for PCR were harvested by TRIzol® Reagent. (Invitrogen, Thermo Fisher, MA, USA, REF: 15596026).

The grouping setting was as following:

	NC	PC	1µmol/ml	5µmol/ml
M-CSF	50ng/ml	50ng/ml	50ng/ml	50ng/ml
RANKL	/	50ng/ml	50ng/ml	50ng/ml
Arcyriafiavin A	/ (8µL DMSO)	/ (8µL DMSO)	1µmol/ml	5µmol/ml

(NC represents Negative control; PC represents Positive control)

TRIzol-Chloroform method was applied to extract total RNA as follows:

Cell Lysis	Adding 1 mL TRIzol® per well		
DNA nhasa	200µL Chloroform (AppliChem GmbH, Germany,		
RNA phase separation	code: A193	35)	
Separation	Centrifugin	g at 11500 rpm, 15min, 4°C	
	500μL 2-Propanol (AppliChem GmbH, Germany, code: A3928)		
RNA precipitation			
	Centrifugin	g at 11500 rpm, 10min, 4°C	
Damask		75 % ethanol (AppliChem GmbH,	
RNA purification	Repeat Twice	Germany, code: A3678)	
Twice		Centrifuging at 9500 rpm, 5min, 4°C	

RNA was standardized to 1000ng/mL and transcribed into single-stranded cDNA. The high-capacity cDNA Reverse Transcription Kit (Applied Biosystems, Thermo Fisher, MA, USA, REF: 4368814) was employed for reverse transcription, and NanoPhotometer® N60 (Implen GmbH, Germany) for RNA concentration measurement and standardization.

PowerUp™ SYBR™ Green Master Mix (Applied Biosystems, Thermo Fisher, MA, USA, Catalog-Nr: A25742) was used as fluorescence probe, and Light-

Cycler® 480II System (Roche, Germany, Serie-Nr: 5363) for gene amplification and fluorescence detection. For quantification, we applied GAPDH as normalization reference, and the $2-\Delta\Delta$ Cq method for analysis.

In the table below we listed the primer sequences:

GENE	FROWARD (5'-3')	REVERSE (5'-3')	Tm (°C)
GAPDH	AGG TCG GTG TGA ACG GAT TTG	TGT AGA CCA TGT AGT TGA GGT	60
NFATc1	GGT GCC TTT TGC GAG CAG TAT C	CGT ATG GAC CAG AAT GTG ACG G	60
c-Fos	GGG AAT GGT GAA GAC CGT GTC A	GCA GCC ATC TTA TTC CGT TCC C	60
TNFrsf11a	GGA CAA CGG AAT CAG ATG TGG TC	CCA CAG AGA TGA AGA GGA GCA C	60
CTSK	CCA GTG GGA GCT ATG GAA GA	AAG TGG TTC ATG GCC AGT TC	60
MMP9	GCT GAC TAC GAT AAG GAC GGC A	TAG TGG TGC AGG CAG AGT AGG A	A 60
DC-stamp	TTT GCC GCT GTG GAC TAT CTG C	GCA GAA TCA TGG ACG ACT CCT T	G60
ACP5	CAG CAG CCA AGG AGG ACT AC	ACA TAG CCC ACA CCG TTC TC	59
Integrin β3	GTG AGT GCG ATG ACT TCT CCT G	CAG GTG TCA GTG CGT GTA GTA C	60
ATP6v0d2	ACG GTG ATG TCA CAG CAG ACG T	CTC TGG ATA GAG CCT GCC GCA	60

In this research, two different types proteins were analyzed. For different purposes, corresponding grouping strategies were established.

For downstream function and differentiation related proteins, same grouping strategy was employed as for the PCR assay (3.0x10⁵ BMMs per well, cultured for 5 days).

The grouping setting was as following:

	NC	PC	1µmol/ml	5µmol/ml
M-CSF	50ng/ml	50ng/ml	50ng/ml	50ng/ml
RANKL	1	50ng/ml	50ng/ml	50ng/ml
Arcyriafiavin A	/ (8µL DMSO)	/ (8µL DMSO)	1µmol/ml	5µmol/ml

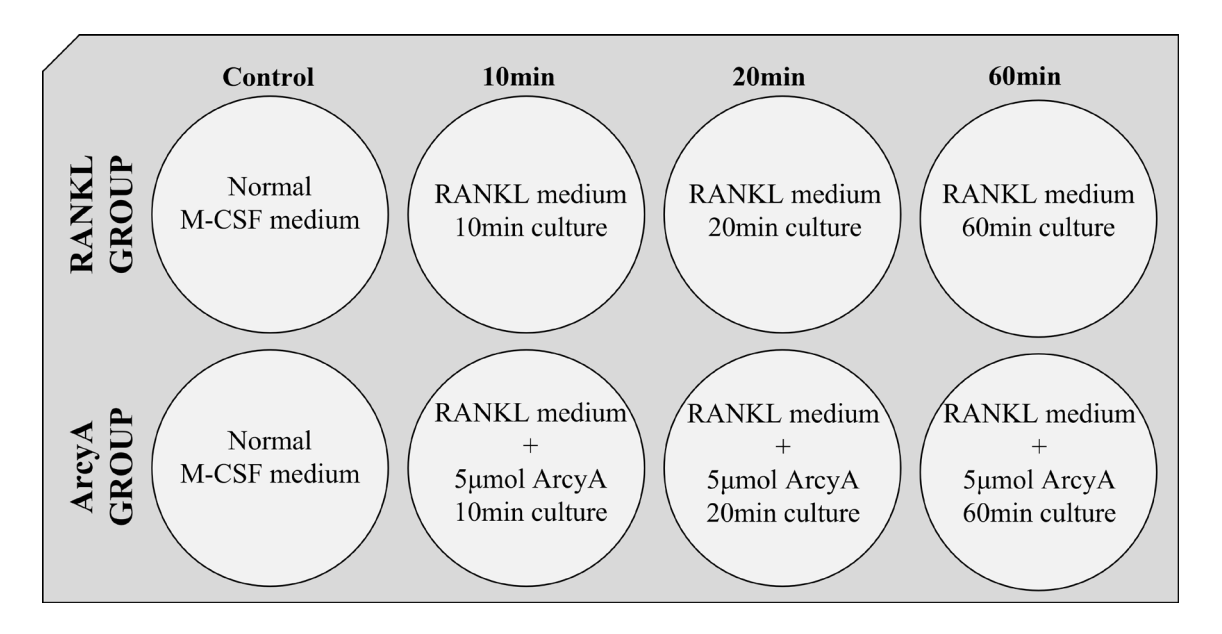
For upstream signaling pathway proteins, we seeded cells in 6-well plates at cell density of 1x10^6 cells. Due to the short duration of the experiment for analyzing upstream signaling proteins, there was not enough time for proliferation, so the larger initial number of cells is essential for sufficient protein

yield. Additionally, the upstream signaling pathway protein exists only for a short time after stimulation. Therefore, the inducing time ought to be limited to in 60min before the degradation of early-stage upstream protein.

For an intuitive presentation of the experimental design, we have listed the process as follows:

Step 1, BMMs were seeded in a 6-well plate, at a density of 1x10^6 cells per well; **Step 2**, BMMs were rested in M-CSF medium for 12h for adhesion and adaptation; **Step 3**, BMMs were starved for 12h using non-serum medium; **Step 4**, BMMs were pretreated with ArcyA for 2h, allowing for ArcyA uptake; **Step 5**, RANKL induction was initiated for 10min, 20min, and 60min.

The grouping and treatment strategy were as following,



The subsequent processing steps of Western-Blot were the same. Cells from different experiments were harvested by RIPA buffer (Carl Roth, Art-Nr: 23T1.1) for total protein collection. Samples were centrifuged for 5min at maximum speed to remove impurities.

The Pierce™ BCA Protein assay kit (Thermo Fisher, MA, USA, REF: 23225) was used for standardizing protein concentrations.

The formula of the protein loading sample was as following,

Standardized protein sample	30µL
Laemmli Sample buffer (Bio-Rad, CA, USA CAT: #1610747)	9µL
2-Mercaptoethanol (AppliChem GmbH, code: A1108)	1µL

^{*}Loading samples were boiled at 95°C for 5min.

The boiled protein samples were separated using 10 % sodium dodecyl sulfate-polyacrylamide gel, and transferred onto nitrocellulose membranes using the Trans-Blot® Turbo™ transfer system (Bio-Rad) subsequently. The blots were detected and imaged using the ChemiDoc Imaging System (Bio-Rad).

Primary anti-bodies were obtained from CST (Cell Signaling Technology, MA, USA), including anti-NFATc1 (D15F1, #8032s, 1:1000); anti-Integrin beta3 (#4702, 1:1000); anti-IkB (L35A5, #4814s, 1:1000); anti-Tubulin (D3U1W, #86298s, 1:5000); anti-GAPDH (D16H11, #5174, 1:5000); and from Invitrogen (Thermo Fisher, MA, USA), including anti-cFos (T.142.5, #MA5-15055); anti-CTSK (Cathepsin K Polyclonal Antibody, #PA5-102483).

Formulars of involved reagents were as follows,

	ı	T T
Blocking Buffer	BSA powder	15g
	10x TBS (Carl Roth, Nr: 1060.1)	50mL
	ddH ₂ 0	Adjust to 500mL
Primary	Blocking Buffer	5mL
Antibody	Tween-20(Carl Roth, Nr: 9127.2)	5µL
Incubation Buffer	Primary Antibody	Given dilution factor
Secondary Antibody	Blocking Buffer	5mL
	Tween-20	5µL
Incubation Buffer	Secondary Antibody	1:10,000
TBST Wash	1x TBS	1000mL
Buffer	Tween-20	1mL
10 % Separating Gel	ddH ₂ O	12.2mL
	30 % Acrylamide/Bis Solution, 29:1	10mL
	pH8.8 Tris HCL (1.5mol/L), 0.4 %SDS	7.5mL
	10 % APS (Carl Roth, Nr: 9592.1)	300µL
	TEMED (Bio-Rad, #1610801)	5µL
	ddH ₂ O	6.8 mL
	30 % Acrylamide/Bis Solution, 29:1	1.7mL
Stacking Gel	pH6.8 Tris HCL (1.0mol/L), 0.1 %SDS	1.25mL
	10 % APS	100µL
	TEMED	2µL

1.2.7 Efficacy test in human cells

Five donors donated whole blood samples for our research. Blood was collected using EDTA-monovettes (Sarstedt, Germany, Nr, 04.1931.010), and diluted with PBS at 1:1 ratio. SepMate[™]-50 tubes (STEMCELL technologies, Canada, REF: 85450) were employed to isolate Peripheral blood mononuclear cells (PBMCs).

We seeded purified PBMCs in 12-well ibidi chambers (Ibidi GmbH, Germany, CAT: 81201) and cultured the cells in human OC induction medium (medium composition are provided later) for 12 days (medium changes every 2 days). In each chamber, the cell density was 5.0x10^5 cells per well, and medium volume was 200µl per well.

The formular of human OC induction medium was as follows,

α-MEM medium for human OC				
human M-CSF (Miltenyi Biotec, Germany, REF 130096491)	50ng/mL			
human RANKL (Miltenyi Biotec, Germany, REF	50ng/mL			
130096494631)				
Vitamin D (Sigma-Aldrich, MA, USA, CAT: 5009360010)	10nM			

The grouping was as following:

	Control	DMSO	0.1µmol/	1µmol/	2.5µmol/	5µmol/
		control	mL	mL	mL	mL
M-CSF	50ng/mL	50ng/mL	50ng/mL	50ng/mL	50ng/mL	50ng/mL
RANKL	50ng/mL	50ng/mL	50ng/mL	50ng/mL	50ng/mL	50ng/mL
ArcyA	1	8µL DMSO	0.1µmol/mL	1µmol/mL	2.5µmol/mL	5µmol/mL

After 12 days, the removable chambers of the ibidi slides were removed, then cells on slides were fixed using 4 % formalin. The same methods as described in the "Phenotype Assay" section were used for TRAP staining and cell counting.

1.2.8 Ovariectomy Mouse Model

To evaluate the alleviating effect of ArcyA in vivo, we established ovariectomy-induced osteoporosis animal models. The design and practice of animal experiments adhered to the 3R principles and ensured welfare of experimental animals.

Fully adapted to the housing environment to preclude stress, twenty 10-week-old female C57BL/6 mice underwent sham operation or bilateral ovarian ligation and resection via the dorsal approach after inhalation isoflurane anesthesia (RWD GmbH, China, CAT: R510-22-16) and skin disinfection.

All mice were placed in a post-anesthesia recovery environment avoiding light and noise exposure. Dosing was initiated after approximately one week after the wound had healed. The frequency of administration was once every five days, and the total duration was eight weeks.

The grouping and intervention schedule was as follows,

	Sham group (n=4)	Sham + ArcyA group (n=4)	Non- treatment group (n=4)	10mg/kg treatment group (n=4)	20mg/kg treatment group (n=4)
OVX	1	1	+	+	+
Saline	+	1	+	1	1
ArcyA	1	20mg/kg	1	10mg/kg	20mg/kg

^{*}All mice involved were obtained from and maintained in the Animal Center of Shanxi Medical University (Shanxi, China).

One tibia from each mouse was extracted after euthanasia after eight-week treatment. Fixed tibiae were scanned using the micro-CT (BRUKER skyscan1176 µCT instrument, Bruker Daltonic Inc. USA). In order to compare the severity of osteoporosis in samples from different groups, the regions of

interest (ROI) were defined in an area 1.8mm in height below the tibial epiphyseal plate. The scanning setup was as follows: 50 kV scanning voltage, 500 µA scanning current, 9 µm spatial resolution, and 1,600 × 2,672-pixel image matrix. The scan results were processed and reconstructed in three-dimension for further quantitative analysis of BV/TV. The software and program for imaging and calculation were NRecon reconstruction software (Ver.2.0) and CTAn (CT-Analyser, Ver.1.18).

1.2.9 Statistical Analysis

Statistical analyses were performed using GraphPad Prism 8 software. Quantitative data are presented as means \pm standard deviation (SD). For comparisons between two groups, an unpaired two-tailed Student's t-test was used. For comparisons among more than two groups, one-way ANOVA followed by Tukey's multiple comparisons test was applied. A p-value less than 0.05 was considered statistically significant. The significance levels are indicated as follows: p < 0.05 (*), p < 0.01 (***), p < 0.001 (****), and p < 0.0001 (*****). The sample size (n) represents the number of independent experimental replicates and is indicated in the respective figure legends.

1.3 Results

1.3.1 Biosafety assay

The CCK8 was employed to evaluate the potential impact of ArcyA to BMMs. The absorbance at OD 450nm, representing cell viability, showed no significant difference between control group and two treatment groups. This result indicated that ArcyA had no cytotoxic effect on BMM growth at concentrations of 1µM and 5µM (Figure 2). Consequently, a potential inhibitory effect of ArcyA on OC differentiation is not attributed to a reduction in BMMs proliferation.

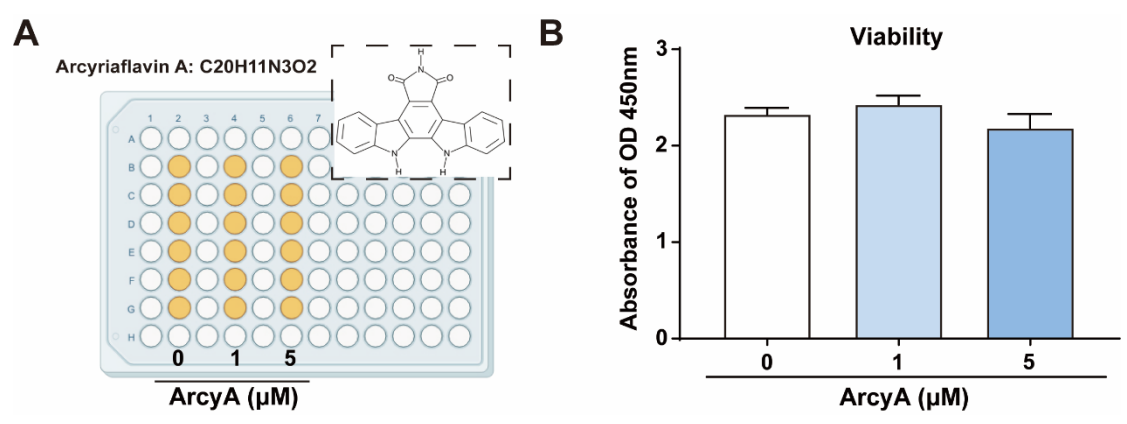


Figure 2. (A) Cell viability assay performed in a 96-well plate and the molecular structure of Arcyriaflavin A (ArcyA). (B) Quantitative analysis of BMMs viability following treatment with ArcyA at concentrations of 0μ M, 1μ M, and 5μ M. N=6 Data are expressed as mean \pm SD. (Modified according to Zhu et al., 2025, The image elements on the left were drawn by BioRender. The molecular structure of Arcyriaflavin A was generated using the InDraw software V6. (https://www.integle.com/static/indraw accessed on 18 July 2025)

1.3.2 Morphology analyses

1.3.2.1 TRAP staining

In the positive control (PC) group, cells differentiated normally, forming many giant multiple nuclei TRAP positive cells. Compared to the PC group, the 1µM ArcyA treatment significantly reduced the number of TRAP-positive cells and precursors (red stained, less than 3 nuclei). The 5µM treatment group demonstrated an even stronger inhibitory effect, with fewer TRAP-positive cells

and OC precursors (Figure 3A). Quantitative analysis revealed that the numbers of TRAP positive cells in both $1\mu M$ and $5\mu M$ groups were significantly lower than the PC group, and the $5\mu M$ group exhibited a more pronounced reduction than the $1\mu M$ group (Figure 3B).

1.3.2.2 Fluorescence staining

The fluorescence staining provided a clearer visualization of OC cells area and nuclei. The results illustrated a significant reduction in the number of giant cells with more than 10 nuclei compared to PC group (Figure 3C). Quantitative analysis further confirmed the concentration-dependency (Figure 3D).

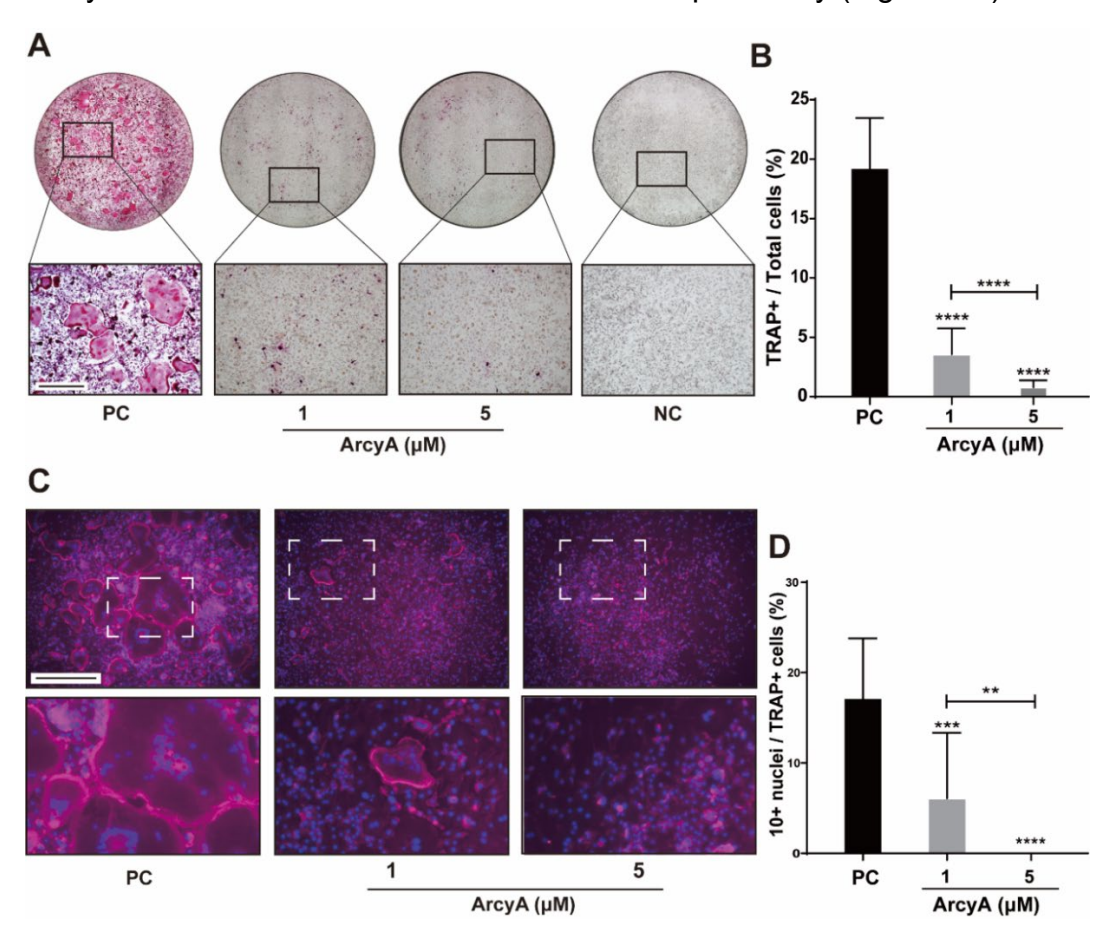


Figure 3. (A) Representative images of TRAP staining of RANKL-induced mouse OCs treated with ArcyA at concentrations of 0 μM (positive control, PC), 1 μM, and 5 μM. Unstained BMMs were used as the negative control (NC). (B) Quantitative analysis of TRAP-positive cell ratio among all cells. (C) Representative images of fluorescence staining of cells treated with ArcyA at concentrations of 0 μM, 1 μM, and 5 μM. (D) Quantitative analysis of the ratios of giant multinucleated cells containing more than 10 nuclei among all multinucleated cells. Scale bar represents 500μm. N=3 Data are

expressed as mean \pm SD, with statistical significance indicated as **P < 0.01, ***P < 0.001, and ****P < 0.0001. (Modified according to Zhu et al., 2025).

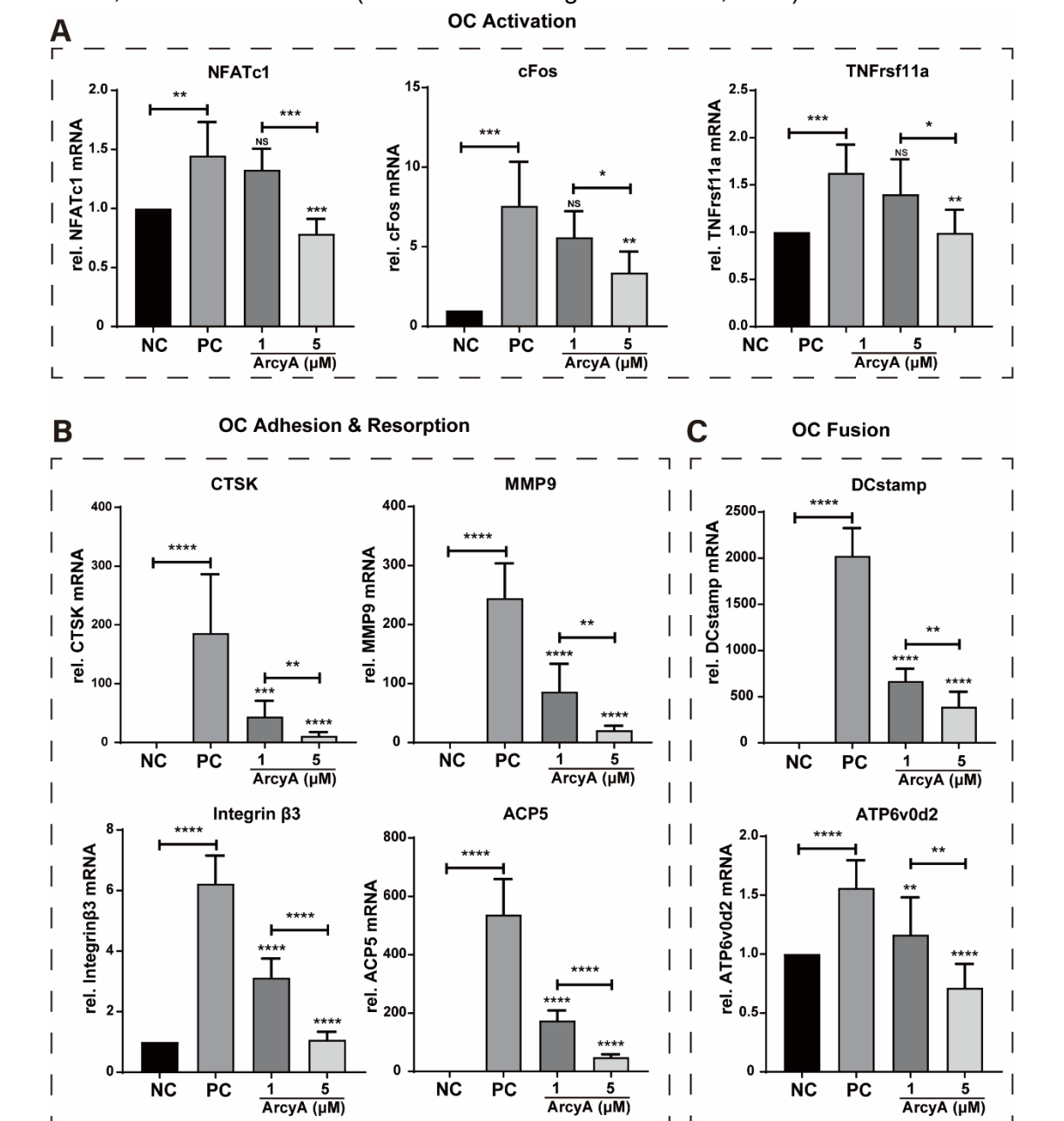


Figure 4. (A) Expression of genes related to osteoclast (OC) activation, including NFATc1, c-Fos, and TNFrs11a, was significantly downregulated by ArcyA at a concentration of 5μ M. There was no significant difference between positive control (PC) group and 1μ M group. (B) Genes associated with OC adhesion and resorption (CTSK, MMP9, Integrin β3, and ACP5) were downregulated by ArcyA at concentrations of 1μ M and 5μ M. (C) Expressions of OC fusion and formation gens (DCstamp and ATP6v0d2) were decreased under the ArcyA treatment at concentrations of 1μ M and 5μ M. Gene expression levels were normalized to GAPDH. N=5. Data are presented as mean \pm SD, with statistical significance indicated as *P<0.05, **P<0.01, ****P<0.001. (Modified according to Zhu et al., 2025).

1.3.3 Molecular analyses

1.3.3.1 PCR

To verify the inhibitory effect of ArcyA at molecular level, we selected 6 genes for analysis, including 3 upstream signaling pathway-related genes: NFATc1, c-Fos, TNFrs11a, and 6 OC formation and function related genes: CTSK, MMP9, integrin β 3, DCstamp, ATP6v0d2, ACP5. The $\Delta\Delta$ CT method was used for calculation. For the upstream signaling pathway genes, no significant differences were observed between the PC group and 1 μ M treatment group. However, the genes were significantly downregulated in both the 1 μ M and 5 μ M treatment groups, with a concentration-dependent inhibitory effect. Significant differences were also observed between the 1 μ M and 5 μ M groups (Figure 4A, B, and C).

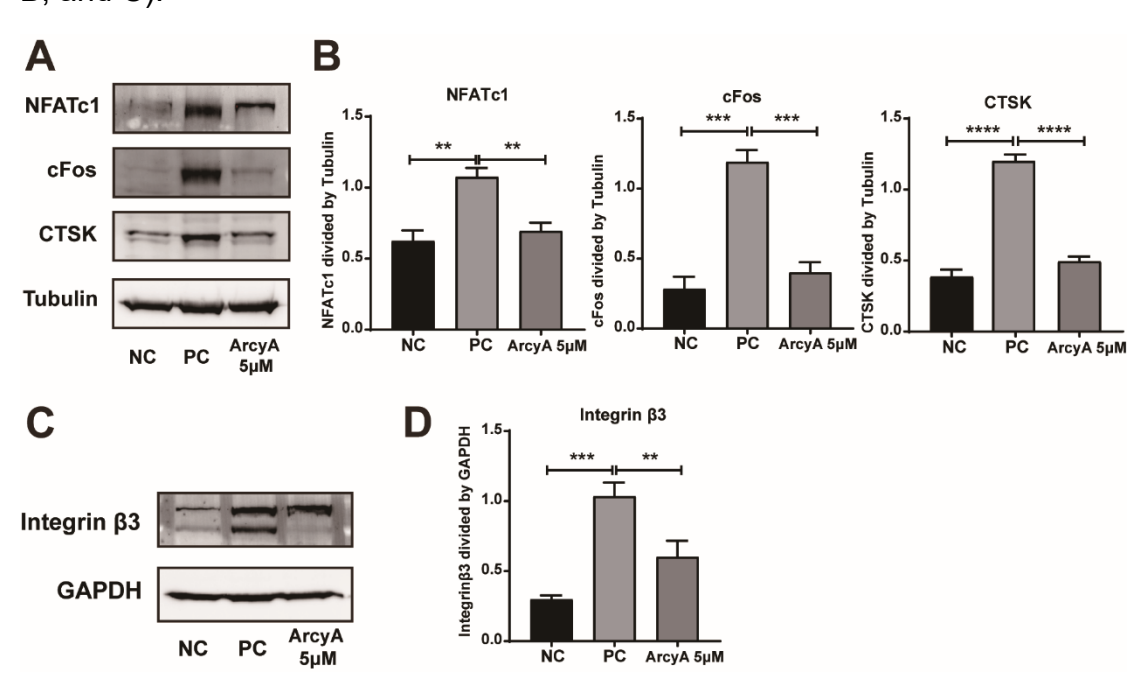


Figure 5. (A) Representative images of blots showing the expression levels of NFATc1, cFos, CTSK in groups of Negative control (NC), Positive control (PC), and 5μ M ArcyA treatment groups. Tubulin served as control. (B) Quantitation of greyscale intensity representing the protein expression level in (A). (C) Blots showing the expression of Integrin β3 in NC, PC and treatment groups. GAPDH served as control. (D) Quantitation of greyscale intensity representing the expressions of Integrin β3. N=3. Data are presented as mean \pm SD, with statistical significance indicated as **P<0.01, ***P<0.001, ****P<0.0001. (Modified according to Zhu et al., 2025).

1.3.3.2 Western Blot

To validate the PCR results at the protein level, we examined 4 representative proteins: NFATc1 and c-Fos, which are key factors for OC differentiation activation as aforesaid; CTSK and integrin β3, which are critical for cells attachment and resorption. Compared to the PC group, the blot of protein bands for all 4 target proteins were lighter in the treatment group (Figure 5A, C). Correspondingly, quantitative analysis supported the results above and echoed our PCR results, suggesting a significantly downregulation in all 4 proteins due to the intervention of ArcyA (Figure 5B, D).

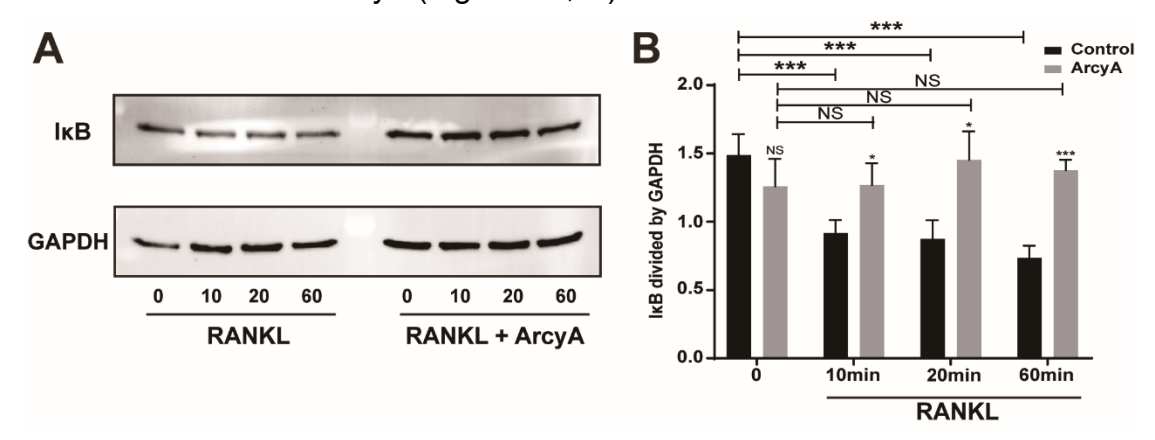


Figure 6. (A) Representative images of blots showing the expression levels of IκB with or without ArcyA pretreatment following RANKL induction at 0, 10, 20, and 60 minutes. (B) Quantitative analysis of IκB expression levels: black bars represent the control group at different time points, while gray bars represent the ArcyA-treated group. N=3. Data are presented as mean ± SD, with statistical significance indicated as *P<0.05, ***P<0.001, ****P<0.0001. (Modified according to Zhu et al., 2025).

1.3.3.3 Early-stage signaling pathway

Protein factors in the NF-κB signaling pathway are not detectable in late stage of OC differentiation. Therefore, protein samples were collected at 10, 20, and 60min after RANKL stimulation. IκB, a critical inhibitory factor against NF-κB pathway activation significantly decreased in the control group at all time points, reflecting the process of IκB phosphorylation and exposure of the phosphorylation site on NF-κB (P65) molecule. In contrast, IκB levels remained stable in the 5μM treatment group, indicating that the ArcyA precluded release

of NF-κB (Figure 6A, B).

1.3.4 Resorption assay

Using apatitic calcium phosphate coated layer 96-well plates, the resorption pits created by OCs were visible under the microscope. In the NC group, we found a black stained, complete coating layer, indicating the absence of OC formation. On the contrary, the PC group showed white resorption pits on a black background due to the coating layer was "eaten" by OCs, exposing the transparent unstainable well bottom. The ratio of resorption pit was calculated using ImageJ. Under a bright-field microscope, we found many irregularly shaped resorption pits in varying sizes. However, in 1µm ArcyA treatment group, the amount and size of resorption pits significantly decreased, while in the 5µm group, the resorption pits were obviously limited (Figure 7A). Quantitative analysis of the resorbed area ratio confirmed that the resorption activity was reduced in both the 1µm and 5µm groups. Furthermore, the high concentration group presented a significantly stronger inhibitory effect on OC resorption (Figure 7B).

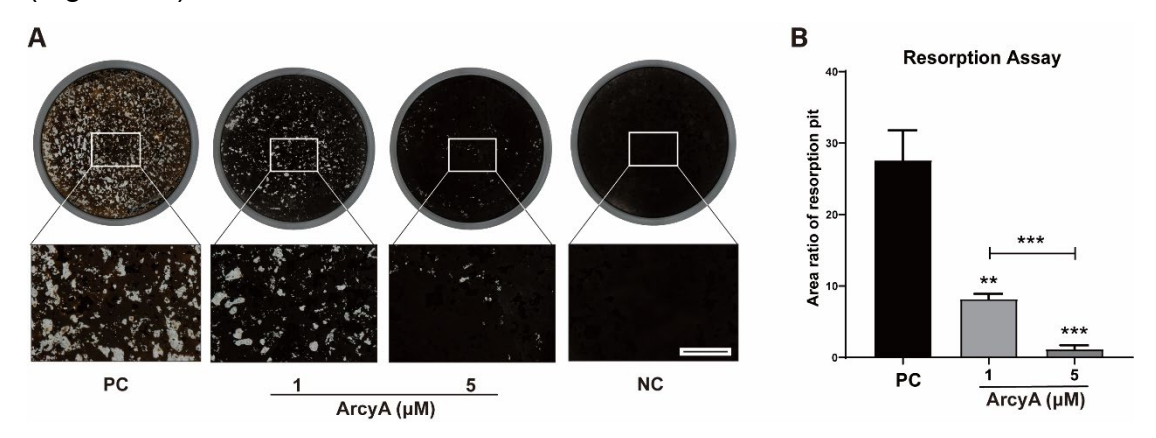


Figure 7. (A) Representative images of resorption pits in positive group (PC), 1μM and 5μM ArcyA treatment groups. Dark area represented remaining coating layer, and the resorption pits appeared white under a bright-field microscope. In the non-RANKL negative group (NC), the coating layer remained intact. (B) Quantitative analysis of the ratio of resorbed area to total well area. Scale bar=500μm. N=3. Data are presented as mean ± SD, with statistical significance indicated as **P<0.01, ***P<0.001. (Cited from Zhu et al., 2025).

1.3.5 Animal experiments

Our in *vitro* findings were confirmed *in vivo*. Tibiae were harvested form 19-week-old female mice. The experimental mice underwent sham operation or bilateral ovarian ligation and resection at 10th week of age, followed by treatment from the 11th week to the 19th week. Micro-CT scanning of proximal tibiae reconstructed a region of 1.8mm height below the tibia epiphyseal plate as the regions of interest (ROI) (Figure 8A). From 3D reconstruction image analysis, we obtained data of BV/TV, reflecting bone density and severity of OP. The data showed no significant difference between sham group and sham + ArcyA group, indicating ArcyA had no adverse effect on normal bone tissue. The untreated OVX group exhibited the lowest bone density, while treatment groups showed a significant increase in bone density in a concentration-dependent manner. Notably, there was no significant difference between the BV/TV value in the 20mg/kg treatment group and sham group (Figure 8B).

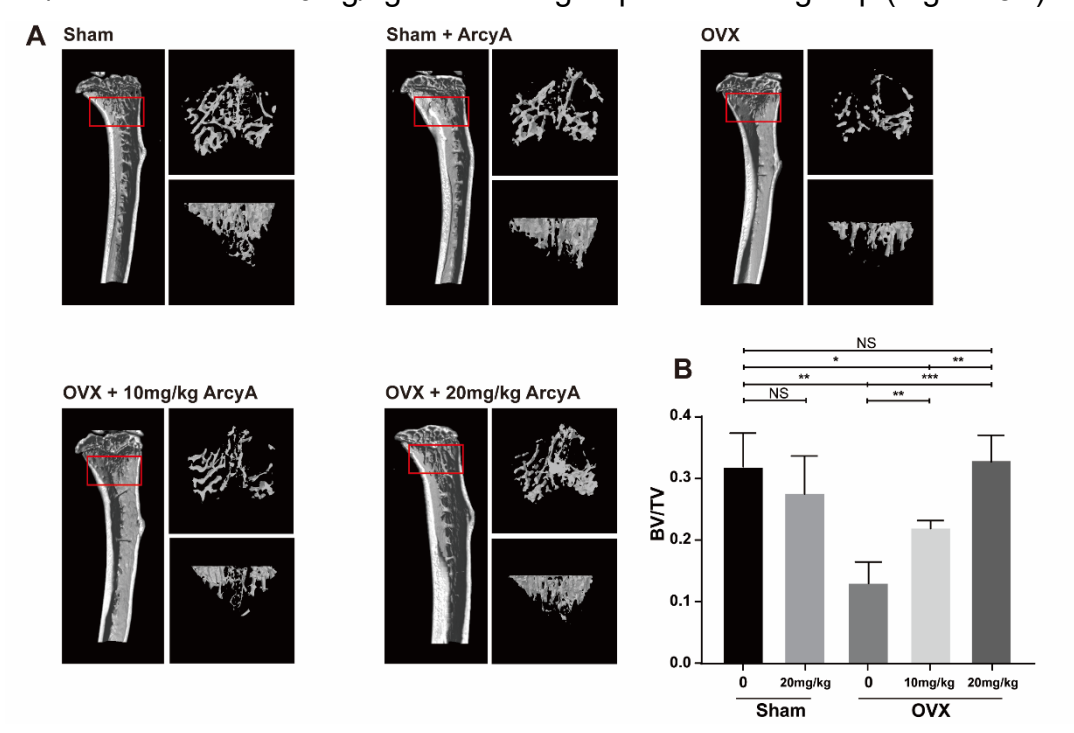


Figure 8. (A) Representative 3D high-resolution micro-CT images of the mice tibiae from a control group (Sham) and four experimental groups. The region of interest (ROI) was defined as a 1.8mm height area below the epiphyseal plate. Enlarged planar and vertical views of ROI were shown. (B) Quantitative data of BV/TV in each group. N=4. Data are presented as mean ± SD, with statistical significance indicated as *P<0.05,

P<0.01, *P<0.001. (Modified according to Zhu et al., 2025).

1.3.6 Human cells

Peripheral blood mononuclear cells (PBMCs) were isolated from peripheral blood donated by five volunteers. Additional treatment groups with ArcyA concentrations of 0.1μM and 2.5μM were included. The number of TRAP positive cells dropped in 0.1μM group, indicating the human OCs were more sensitive to ArcyA than mouse cells, and OC differentiation was significantly suppressed at higher concentration (1μM, 2.5μM, 5μM) (Figure 8A). The quantitative TRAP positive cells counting supported the observation above. There was no significant difference between DMSO control and control, ruling out the influence of DMSO to OC differentiation. In general, the inhibitory effect of ArcyA on human OC is concentration-dependent. However, the suppressing effect of 1μM AcryA was not distinct from 2.5μM (Figure 8B).

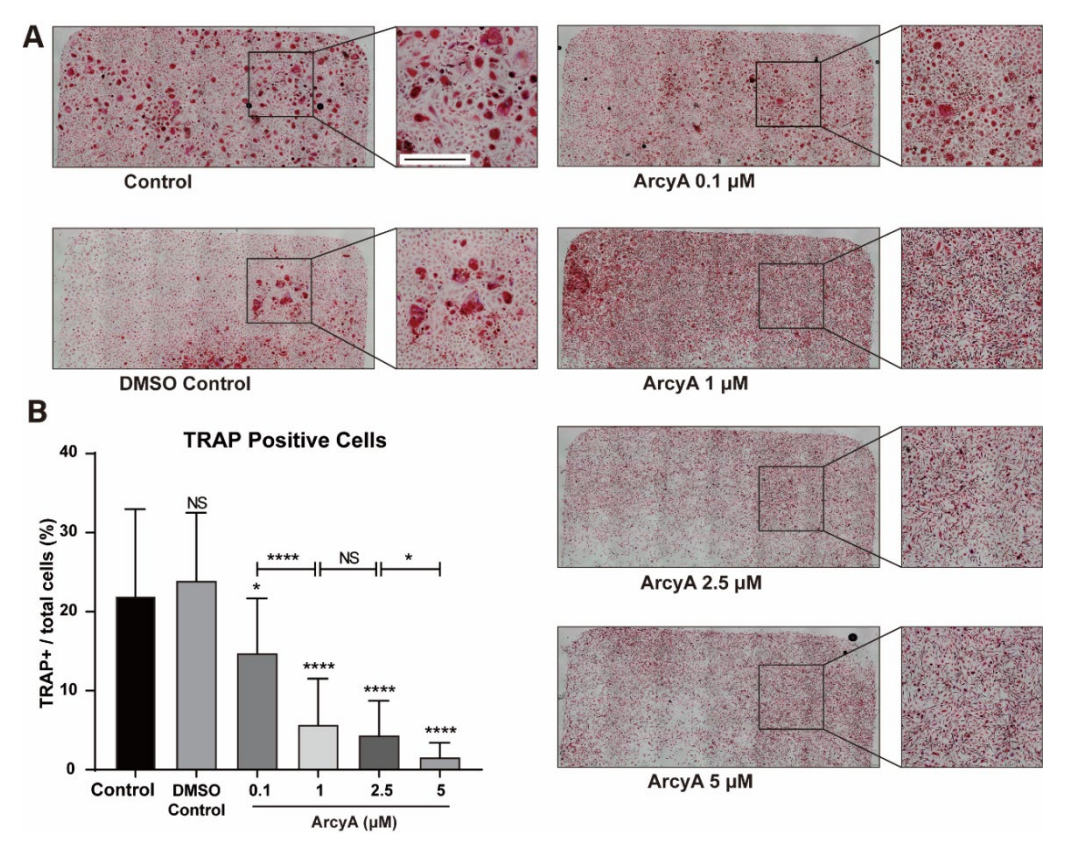


Figure 9. (A) Representative images of TRAP staining of RANKL-induced human OCs treated with ArcyA at concentrations of 0μ M (control), 1μ M, 2.5μ M and 5μ M. Cells treated with DMSO only was defined as DMSO control (B) Quantitative analysis of TRAP-positive cell ratio among all cells. Scale bar=500 μ m. N=4. Data are expressed

as mean \pm SD, with statistical significance indicated as *P < 0.05, and ****P < 0.0001. (Modified according to Zhu et al., 2025).

1.4 Discussion

Derived from hematopoietic stem cells (HSCs), OCs play a critical role in bone microenvironment metabolism by removing obsolete and damaged bone through the secretion of proteolytic enzymes and hydrogen ions to degrade bone tissue (Asagiri et al., 2007, Boyle et al., 2003, Feng et al., 2013, Kim, et al. 2020). OC precursors are recruited into the "bone remodeling compartment" (BRC), where they further differentiate to functional mature OCs (precursors of osteoblast are also immigrated into BRC for bone formation) (Martin et al., 2007). Notably, this anatomical entity, enclosed by flat cells, is where bone resorption and formation are coupled (Andersen, et al. 2009). In this microenvironment, OC precursors are regulated by cytokines and eventually mature into functional OCs.

Macrophage colony stimulating factor (M-CSF) is indispensable for the maturation of BMMs, driving the differentiation of macrophage progenitors into macrophage, which serve as the OC precursors. (Metcalf 2008)Furthermore, the existence of M-CSF is necessary for OC precursors to sustain their proliferative activity and differentiation potential (Mun et al., 2020). MC-CSF also facilities the re-arrangement of cytoskeleton, cells migration and fusion, contributing to formation of giant multiple nuclei cells (MNCs) (Faccio et al., 2007). Thus, we applied M-CSF in the medium from the initial stage to the telophase of OC differentiation.

For the further OC differentiation, the co-existence of M-CSF and Receptor Activator of NF-κB Ligand (RANKL) is indispensable. RANKL, the cognate ligand of Receptor Activator of NF-κB (RANK), is essential for enabling the OC to achieve its function by upregulating downstream related genes and proteins

(Asagiri, et al. 2007, Boyle, et al. 2003). Additionally, RANKL promotes mitochondrial biogenesis, enhancing energy transfer via electron transport chain (ETC) to sustain the metabolism for maintaining giant morphology of OCs (Asagiri, et al. 2007, Da et al., 2021). Together with osteoprotegerin (OPG), RANKL and RANK form a negative feedback regulation axis that maintains homeostasis in the bone microenvironment. OPG acts as a competitive inhibitor against RANKL preventing its interaction with RANK (Udagawa et al., 2021). Previous studies have identified postmenopausal estrogen deficiency as a major trigger of osteoporosis in elderly females (Riggs et al., 2002). Mechanistically, estrogen insufficiency led to an increased number of T and B cells expressing RANKL, which subsequently results in overactivity of OCs (Eghbali-Fatourechi et al., 2003, Onal et al., 2012). Given that, it is considered RANKL is one of the most significant target molecules for therapeutic intervention, which is the reason why we selected RANKL induced cell models as our research objects.

However, RANKL is not derived from a single source, nor is OC overactivation attributable to a single factor. In addition to osteoblasts, dendritic cells, fibroblasts, T cells, bone marrow stromal cells (BMSC) produce RANKL as well (Asagiri, et al. 2007, Boyle, et al. 2003, Feng, et al. 2013). Given the substantial overlap between RANKL-releasing cells and proinflammatory cells, OC differentiation can be closely linked to systemic inflammation, explaining reasonably the correlation of OP and inflammation. OP often arises in the context of chronic systemic inflammation and is triggered by multiple contributing factors. It could be an explanation why OP usually manifests as a complication of immunocompromising conditions, including but not limited to cancer, anemia, COPD, overweight, malnutrition, and chronic kidney disease (Johnston et al., 2020, Li et al., 2022, Liu et al., 2023, Pazianas et al., 2021, Yang et al., 2023). Therefore, we need to view the OC overactivation and OP with a comprehensive eyesight. From the standpoint of systematic inflammation,

macrophage polarization is an unignorable role.

Numerous previous studies revealed the complex relation between macrophage polarization and OC differentiation. Macrophage polarization regulates OC differentiation through multiple pathways. By releasing cytokines, M1 macrophage polarization creates an OC-promoting microenvironment. In the microenvironment of bone reconstruction and resorption, M1 macrophages (usually induced by LPS, TNF α , and IFN- γ) release inflammatory factors, such as IL-12, IL-6, and IL-1, promoting OC differentiation and function. In contrast, M2 macrophages, primarily induced by IL-4 from immune-conditioning cells (e.g., PTH, CD4+ T cells), exert an opposite effect. M2 macrophages release cytokines, such as TGF- β , IL-18, and IL-10, which suppress the OC formation (Hu, et al. 2023, Kim, et al. 2009, Munoz, et al. 2020, Piek et al., 2001, Souza, et al. 2013).

A recent study reported that M2 macrophages could influence the OC differentiation by releasing exosomes, commonly referred to as extracellular vesicles (EVs). These M2 EVs reduce both the number and function of OCs through reversing OC precursors to M2 macrophages (Huang et al., 2024).

Regarding macrophage polarization, Hu et al. previously mentioned various drugs as M2 polarization activators. Through screening, we identified Arcyriaflavin A (ArcyA) as a potential osteoclast inhibitor (Hu, et al. 2021). ArcyA is a typical natural indolocarbazole compound derived from slime molds and marine invertebrates (Bitzenhofer et al., 2023). Although research on ArcyA remains limited, former studies have reported that it functions as an inhibitor of cyclin D1-cyclin-dependent kinase 4 (CDK4), thereby reducing viability and proliferation of endometriotic cyst stromal cells (ECSCs) (Hoshino et al., 2015). The inhibitory effect of ArcyA on CDK4 caught our attention, as it may provide insights into the potential mechanism underlying ArcyA-induced M2 activation.

In the immune microenvironment, M2 macrophage polarization is regulated by the JAK-STAT3-IL6 axis. Upon JAK activation, the cytoplasmic protein STAT3 undergoes phosphorylation, dimerization, and nuclear-translocation, leading to the activation of downstream genes expression, including IL-6, a well-known cytokine that promotes M2 polarization. This signaling process occurs in monocytes, macrophages, fibroblasts, T cells, B cells, and endothelial cells (Bienvenu et al., 2001, Hu et al., 2024, Johnson et al., 2018, Lee et al., 2023, Yan et al., 2022). Here could be a possible explanation: By inhibiting CDK4, a suppressor of the JAK-STAT3-IL6 axis, ArcyA indirectly facilitates M2 polarization (Figure 10).

The supporting evidence presented above further motivated us to explore the OC-inhibitory effect of ArcyA in greater depth. The tartrate resistant acid phosphatase (TRAP) staining is what we utilized on our cell model to assess whether out intervention exerted an inhibitory effect to the cell models. TRAP, a member of acid phosphatase family, is specifically expressed in OCs (Bull et al., 2002, Hayman et al., 2003). Therefore, the cytoplasm of MNCs and OC precursors with the potential for further differentiation stains red, creating a sharp contrast with the unstained undifferentiated BMMs. The significant reduction in the number of TRAP positive cells in the ArcyA treatment groups demonstrated the inhibitory effect of the intervention. This staining method was also employed as a screening tool to identify potential inhibitors from candidate compounds.

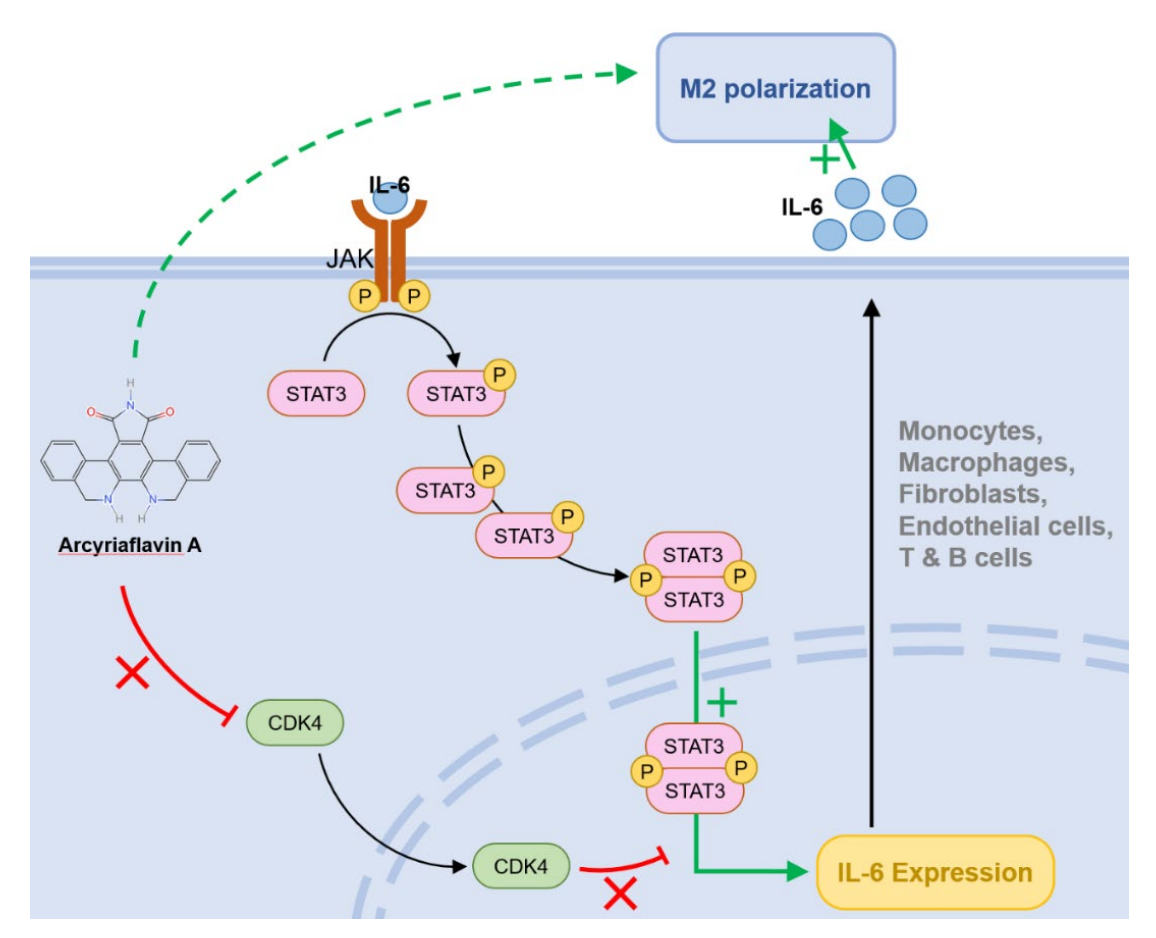


Figure 10: JAK-STAT3-IL6 axis. The receptor of JAK on M2 macrophages can be stimulated by IL-6 released by itself. CDK4 acts as a break of this positive feedback regulation. By inhibiting the phosphorylation of STAT3, CDK4 prohibits the dimerized STAT3-inducing upregulation of downstream genes. The image is drawn using Microsoft Office PowerPoint. The molecular structure of Arcyriaflavin A was generated using the InDraw software V6. (https://www.integle.com/static/indraw accessed on 18 July 2025)

Based on the TRAP staining results, we conducted additional molecular-level assays to validate the reliability of our screening outcomes. A series of genes were selected for comprehensive analysis of OC differentiation and function. Nuclear factor of activated T cells c1 (NFATc1) serves as the master regulator of differentiation. Activated by RANKL-NF-kB signaling and Ca2+ signaling, NFATc1 undergoes auto-amplification and further activates downstream functional genes. During this auto-amplification process, c-Fos is a critical component recruited to NFATc1, mediating the combination between the RANKL-RANK complex and NFATc1. Additionally, RANK, the membrane

receptor of RANKL, is encoded by the TNFrs11a gene (Asagiri et al., 2005, Kim et al., 2014, Negishi-Koga et al., 2009). Based on this, we selected three regulative genes – NFATc1, c-Fos, and TNFrs11a – as the target parameters to assess the impact of ArcyA on OC differentiation.

Furthermore, six additional downstream genes were analyzed to evaluate the inhibitory effects of ArcyA from various perspectives. Regarding the primary resorptive function of OCs, the biological activities include the formation of sealed resorptive zones between MNCs and bone surface, as well as the secretion of proteinases. The attachment of MNCs to the bone surface is mediated by Integrin β3; while MMP9 and CTSK encoding corresponding proteinases responsible for extracellular matrix (ECM) degradation (Drake et al., 2017, Geoghegan et al., 2019, Huang 2018, Nakamura et al., 2003). The formation of MNCs, acritical step for OC function, is regulated by DC-stamp and ATP6v0d2. These proteins are the major regulators of cell-fusion. The downregulation of the two corresponding genes inhibits the formation of MNCs (Chiu et al., 2016, Lee et al., 2006). Besides, ACP5, which encodes tartrateresistant acid phosphatase, was also included in the analysis (Kirstein et al., 2006). To corroborate the gene expression data, we further evaluated the expression levels of representative proteins, including NFATc1, c-Fos, CTSK, and integrin β3, using Western-Blot analysis. The results from Western-Blot were consistent with our finding in PCR, reinforcing the reliability of conclusions.

As a bridge of interaction between RANKL-RANK and NFATc1 activation, the NF-κB signaling pathway in the cytoplasm plays an unignorable role in transmitting signals from the cell membrane to the nucleus. IκB blocks the phosphorylation site of NF-κB (p65), prohibiting the generation of phosphorylated NF-κB (p-p65) which is capable of translocating into the nucleus (Ghosh et al., 2002, Hayden et al., 2004). Our results demonstrated that ArcyA treatment increased the IκB level during the initial stage of

RANKL
RANK

P65

RANK

P65

Arcyriaflavin A

OC differentiation / function

differentiation, precluding signal transmission towards the nucleus.

Figure 11: The pattern graph of NFκB signaling pathway indicating the special inhibitory rola of iκB in the pathway. By blocking the phosphorylation site of P65 molecule (NF-κB), iκB prohibits the into-nucleus translocation of P65 molecule, and further inhibits the activation of NFκB pathway. The image is drawn using Microsoft Office PowerPoint. The molecular structure of Arcyriaflavin A was generated using the InDraw software V6. (https://www.integle.com/static/indraw accessed on 18 July 2025) (Cited from Zhu et al., 2025).

NFATc1

MMP9 DCstamp

Integrin β3 ATP6v0d2 ACP5

These intriguing molecular-level findings encouraged to investigate the inhibitory effect of ArcyA on OC resorptive function. Following the method of Tas and Buhaduri (Tas et al., 2004), our results aligned with the corresponding expectations. Results from animal experiments further supported abovementioned findings, demonstrating that ArcyA alleviated osteoporosis in ovariectomy mice. Additionally, experiments on human cells treated with ArcyA corroborated these results and highlighted the broader potential applications of ArcyA in therapeutic contexts.

While our study provides important insights, much remains to be explored in this field, and future investigations will be essential to build upon our findings. More and more studies believe that the OC differentiation is rather a reversable 41

dynamic than a linear process. In the microenvironment of OC differentiation, multiple cells, including BMMs, OC precursors, polarized macrophages coexistent. Further experiments, including flow cytometry, could help to provide deeper insights into the change of ratios of various cells related to OC differentiation in the context of ArcyA intervention. Bioinformatics could also contribute to uncover more potential mechanisms by analyzing differentially expressed genes.

Especially, the bioenergetics of osteoclastogenesis has become a current hotspot, sparking a wide range of opinions. OC differentiation results in an increased energy demand to sustain the giant cell morphology and active function. The in resorption changes energy requirements osteoclastogenesis involve various potential mechanisms, including but not limited to anaerobic and aerobic glycolysis, as well as alterations in the number and morphology of mitochondria. Currently, a comprehensive idea of OC metabolism is absent. Some studies reported that OCs exhibit a higher Oxygen Consumption Rate (OCR), particularly in the non-mitochondrial respiration, which is greater than that in OC precursors and macrophages. This suggests a higher level of anaerobic glycolysis in OCs. Other research has indicated that M2 macrophages can influence the energy metabolism of OC precursors by transferring glutamine and α-ketoglutarate, which are essential for the tricarboxylic acid cycle (TAC) (Huang, et al. 2024, Ledesma-Colunga et al., 2023, Li et al., 2020, Liu et al., 2023). These exciting findings bring us valuable ideas for our future plan. By comparing the treatment group with the control group at different time points, we can analyze changes in the cellular energy metabolism and differences in metabolic products. This metabolic profiling would allow a deeper understanding of the mechanism of the therapeutic effect of the drug, furthermore, may reveal additional potential regulatory targets. Such analysis not only provides a more comprehensive view of the pharmacological properties of the treatment, but also contributes to expanding

our knowledge of OC differentiation.

1.5 Summary

This study discovered a novel, previously unreported drug, Arcyriaflavin A, which inhibits osteoclast formation in an *in vitro* mouse osteoclast model. The inhibitory effects were validated from multiple perspectives. Additionally, the study further confirmed the drug's inhibitory effects on osteoclasts in OVX animal osteoporosis models and human cells. Since ArcyA itself is a compound capable of influencing the polarization of M0 macrophages towards the M2 phenotype, it also suggests a potential connection between macrophage polarization and the development of osteoporosis.

1.6 References

Alsoof, D., Anderson, G., McDonald, C. L., Basques, B., Kuris, E. and Daniels, A. H. Diagnosis and Management of Vertebral Compression Fracture. Am J Med. 2022; 135: 815-821

Andersen, T. L., Sondergaard, T. E., Skorzynska, K. E., Dagnaes-Hansen, F., Plesner, T. L., Hauge, E. M., Plesner, T. and Delaisse, J. M. A physical mechanism for coupling bone resorption and formation in adult human bone. Am J Pathol. 2009; 174: 239-247

Asagiri, M., Sato, K., Usami, T., Ochi, S., Nishina, H., Yoshida, H., Morita, I., Wagner, E. F., et al. Autoamplification of NFATc1 expression determines its essential role in bone homeostasis. J Exp Med. 2005; 202: 1261-1269

Asagiri, M. and Takayanagi, H. The molecular understanding of osteoclast differentiation. Bone. 2007; 40: 251-264

Assouline-Dayan, Y., Chang, C., Greenspan, A., Shoenfeld, Y. and Gershwin, M. E. Pathogenesis and natural history of osteonecrosis. Semin Arthritis Rheum. 2002; 32: 94-124

Bautmans, I., Knoop, V., Amuthavalli Thiyagarajan, J., Maier, A. B., Beard, J. R., Freiberger, E., Belsky, D., Aubertin-Leheudre, M., et al. WHO working definition of vitality capacity for healthy longevity monitoring. Lancet Healthy Longev. 2022; 3: e789-e796

Bienvenu, F., Gascan, H. and Coqueret, O. Cyclin D1 represses STAT3 activation through a Cdk4-independent mechanism. J Biol Chem. 2001; 276: 16840-16847

Bitzenhofer, N. L., Classen, T., Jaeger, K. E. and Loeschcke, A. Biotransformation Of I-Tryptophan To Produce Arcyriaflavin A With Pseudomonas putida KT2440. Chembiochem. 2023; 24: e202300576

Boyle, W. J., Simonet, W. S. and Lacey, D. L. Osteoclast differentiation and activation. Nature. 2003; 423: 337-342

Bull, H., Murray, P. G., Thomas, D., Fraser, A. M. and Nelson, P. N. Acid phosphatases. Mol Pathol. 2002; 55: 65-72

Chiu, Y. H. and Ritchlin, C. T. DC-STAMP: A Key Regulator in Osteoclast Differentiation. J Cell Physiol. 2016; 231: 2402-2407

Clynes, M. A., Harvey, N. C., Curtis, E. M., Fuggle, N. R., Dennison, E. M. and Cooper, C. The epidemiology of osteoporosis. Br Med Bull. 2020; 133: 105-117

Da, W., Tao, L. and Zhu, Y. The Role of Osteoclast Energy Metabolism in the Occurrence and Development of Osteoporosis. Front Endocrinol (Lausanne). 2021; 12: 675385

Drake, M. T., Clarke, B. L., Oursler, M. J. and Khosla, S. Cathepsin K Inhibitors for Osteoporosis: Biology, Potential Clinical Utility, and Lessons Learned. Endocr Rev. 2017; 38: 325-350

Eghbali-Fatourechi, G., Khosla, S., Sanyal, A., Boyle, W. J., Lacey, D. L. and Riggs, B. L. Role of RANK ligand in mediating increased bone resorption in early postmenopausal women. J Clin Invest. 2003; 111: 1221-1230

European Prospective Osteoporosis Study, G., Felsenberg, D., Silman, A. J.,

Lunt, M., Armbrecht, G., Ismail, A. A., Finn, J. D., Cockerill, W. C., et al. Incidence of vertebral fracture in europe: results from the European Prospective Osteoporosis Study (EPOS). J Bone Miner Res. 2002; 17: 716-724

Faccio, R., Takeshita, S., Colaianni, G., Chappel, J., Zallone, A., Teitelbaum, S. L. and Ross, F. P. M-CSF regulates the cytoskeleton via recruitment of a multimeric signaling complex to c-Fms Tyr-559/697/721. J Biol Chem. 2007; 282: 18991-18999

Feng, X. and Teitelbaum, S. L. Osteoclasts: New Insights. Bone Res. 2013; 1: 11-26

Funck-Brentano, T. and Cohen-Solal, M. Crosstalk between cartilage and bone: when bone cytokines matter. Cytokine Growth Factor Rev. 2011; 22: 91-97

Geoghegan, I. P., Hoey, D. A. and McNamara, L. M. Integrins in Osteocyte Biology and Mechanotransduction. Curr Osteoporos Rep. 2019; 17: 195-206

Ghosh, S. and Karin, M. Missing pieces in the NF-kappaB puzzle. Cell. 2002; 109 Suppl: S81-96

Harvey, N., Dennison, E. and Cooper, C. Osteoporosis: impact on health and economics. Nat Rev Rheumatol. 2010; 6: 99-105

Hayden, M. S. and Ghosh, S. Signaling to NF-kappaB. Genes Dev. 2004; 18: 2195-2224

Hayman, A. R. and Cox, T. M. Tartrate-resistant acid phosphatase knockout mice. J Bone Miner Res. 2003; 18: 1905-1907

Hoshino, S., Zhang, L., Awakawa, T., Wakimoto, T., Onaka, H. and Abe, I. Arcyriaflavin E, a new cytotoxic indolocarbazole alkaloid isolated by combined-culture of mycolic acid-containing bacteria and Streptomyces cinnamoneus NBRC 13823. J Antibiot (Tokyo). 2015; 68: 342-344

Hu, G., Su, Y., Kang, B. H., Fan, Z., Dong, T., Brown, D. R., Cheah, J., Wittrup, K. D., et al. High-throughput phenotypic screen and transcriptional analysis identify new compounds and targets for macrophage reprogramming. Nat Commun. 2021; 12: 773

Hu, K., Shang, Z., Yang, X., Zhang, Y. and Cao, L. Macrophage Polarization and the Regulation of Bone Immunity in Bone Homeostasis. J Inflamm Res. 2023; 16: 3563-3580

Hu, Z., Sui, Q., Jin, X., Shan, G., Huang, Y., Yi, Y., Zeng, D., Zhao, M., et al. IL6-STAT3-C/EBPbeta-IL6 positive feedback loop in tumor-associated macrophages promotes the EMT and metastasis of lung adenocarcinoma. J Exp Clin Cancer Res. 2024; 43: 63

Huang, H. Matrix Metalloproteinase-9 (MMP-9) as a Cancer Biomarker and MMP-9 Biosensors: Recent Advances. Sensors (Basel). 2018; 18: Huang, X., Lan, Y., Shen, J., Zhao, X., Zhou, Y., Wu, W., Mao, J., Wu, Y., et al. M2 macrophages secrete glutamate-containing extracellular vesicles to alleviate osteoporosis by reshaping osteoclast precursor fate. Mol Ther. 2024;

32: 1158-1177

Johnson, D. E., O'Keefe, R. A. and Grandis, J. R. Targeting the IL-6/JAK/STAT3 signalling axis in cancer. Nat Rev Clin Oncol. 2018; 15: 234-248

Johnston, C. B. and Dagar, M. Osteoporosis in Older Adults. Med Clin North

Am. 2020; 104: 873-884

Kanis, J. A., McCloskey, E. V., Johansson, H., Cooper, C., Rizzoli, R., Reginster, J. Y., Scientific Advisory Board of the European Society for, C., Economic Aspects of, O., et al. European guidance for the diagnosis and management of osteoporosis in postmenopausal women. Osteoporos Int. 2013; 24: 23-57

Katsimbri, P. The biology of normal bone remodelling. Eur J Cancer Care (Engl). 2017; 26:

Khan, A. A., Morrison, A., Hanley, D. A., Felsenberg, D., McCauley, L. K., O'Ryan, F., Reid, I. R., Ruggiero, S. L., et al. Diagnosis and management of osteonecrosis of the jaw: a systematic review and international consensus. J Bone Miner Res. 2015; 30: 3-23

Kim, J. H., Jin, H. M., Kim, K., Song, I., Youn, B. U., Matsuo, K. and Kim, N. The mechanism of osteoclast differentiation induced by IL-1. J Immunol. 2009; 183: 1862-1870

Kim, J. H. and Kim, N. Regulation of NFATc1 in Osteoclast Differentiation. J Bone Metab. 2014; 21: 233-241

Kim, J. M., Lin, C., Stavre, Z., Greenblatt, M. B. and Shim, J. H. Osteoblast-Osteoclast Communication and Bone Homeostasis. Cells. 2020; 9:

Kirstein, B., Chambers, T. J. and Fuller, K. Secretion of tartrate-resistant acid phosphatase by osteoclasts correlates with resorptive behavior. J Cell Biochem. 2006; 98: 1085-1094

Lamy, O., Stoll, D., Aubry-Rozier, B. and Rodriguez, E. G. Stopping Denosumab. Curr Osteoporos Rep. 2019; 17: 8-15

Lane, N. E. Epidemiology, etiology, and diagnosis of osteoporosis. Am J Obstet Gynecol. 2006; 194: S3-11

Le Dare, B., Lagente, V. and Gicquel, T. Ethanol and its metabolites: update on toxicity, benefits, and focus on immunomodulatory effects. Drug Metab Rev. 2019; 51: 545-561

LeBoff, M. S., Greenspan, S. L., Insogna, K. L., Lewiecki, E. M., Saag, K. G., Singer, A. J. and Siris, E. S. The clinician's guide to prevention and treatment of osteoporosis. Osteoporos Int. 2022; 33: 2049-2102

Ledesma-Colunga, M. G., Passin, V., Lademann, F., Hofbauer, L. C. and Rauner, M. Novel Insights into Osteoclast Energy Metabolism. Curr Osteoporos Rep. 2023; 21: 660-669

Lee, H. J. and Hoe, H. S. Inhibition of CDK4/6 regulates AD pathology, neuroinflammation and cognitive function through DYRK1A/STAT3 signaling. Pharmacol Res. 2023; 190: 106725

Lee, S. H., Gong, H. S., Kim, T. H., Park, S. Y., Shin, J. H., Cho, S. W. and Byun, D. W. Position Statement: Drug Holiday in Osteoporosis Treatment with Bisphosphonates in South Korea. J Bone Metab. 2015; 22: 167-174

Lee, S. H., Rho, J., Jeong, D., Sul, J. Y., Kim, T., Kim, N., Kang, J. S., Miyamoto, T., et al. v-ATPase V0 subunit d2-deficient mice exhibit impaired osteoclast fusion and increased bone formation. Nat Med. 2006; 12: 1403-1409

Li, B., Lee, W. C., Song, C., Ye, L., Abel, E. D. and Long, F. Both aerobic glycolysis and mitochondrial respiration are required for osteoclast differentiation. FASEB J. 2020; 34: 11058-11067

Li, M., Zhang, Z. L., Liao, E. Y., Chen, D. C., Liu, J., Tao, T. Z., Wu, W., Xia, W. B., et al. Effect of low-dose alendronate treatment on bone mineral density and bone turnover markers in Chinese postmenopausal women with osteopenia and osteoporosis. Menopause. 2013; 20: 72-78

Li, Y., Gao, H., Zhao, L. and Wang, J. Osteoporosis in COPD patients: Risk factors and pulmonary rehabilitation. Clin Respir J. 2022; 16: 487-496

Liu, H., Zhai, L., Liu, Y., Lu, D., Vander Ark, A., Yang, T. and Krawczyk, C. M. The histone demethylase KDM5C controls female bone mass by promoting energy metabolism in osteoclasts. Sci Adv. 2023; 9: eadg0731

Liu, Y., Liu, Y., Huang, Y., Le, S., Jiang, H., Ruan, B., Ao, X., Shi, X., et al. The effect of overweight or obesity on osteoporosis: A systematic review and meta-analysis. Clin Nutr. 2023; 42: 2457-2467

Martin, T. J. and Seeman, E. New mechanisms and targets in the treatment of bone fragility. Clin Sci (Lond). 2007; 112: 77-91

Metcalf, D. Hematopoietic cytokines. Blood. 2008; 111: 485-491

Mun, S. H., Park, P. S. U. and Park-Min, K. H. The M-CSF receptor in osteoclasts and beyond. Exp Mol Med. 2020; 52: 1239-1254

Munoz, J., Akhavan, N. S., Mullins, A. P. and Arjmandi, B. H. Macrophage Polarization and Osteoporosis: A Review. Nutrients. 2020; 12:

Nakamura, I., Rodan, G. A. and Duong, L. T. Regulatory mechanism of osteoclast activation. J Electron Microsc (Tokyo). 2003; 52: 527-533

Negishi-Koga, T. and Takayanagi, H. Ca2+-NFATc1 signaling is an essential axis of osteoclast differentiation. Immunol Rev. 2009; 231: 241-256

Oleksik, A., Lips, P., Dawson, A., Minshall, M. E., Shen, W., Cooper, C. and Kanis, J. Health-related quality of life in postmenopausal women with low BMD with or without prevalent vertebral fractures. J Bone Miner Res. 2000; 15: 1384-1392

Onal, M., Xiong, J., Chen, X., Thostenson, J. D., Almeida, M., Manolagas, S. C. and O'Brien, C. A. Receptor activator of nuclear factor kappaB ligand (RANKL) protein expression by B lymphocytes contributes to ovariectomy-induced bone loss. J Biol Chem. 2012; 287: 29851-29860

Pazianas, M. and Miller, P. D. Osteoporosis and Chronic Kidney Disease-Mineral and Bone Disorder (CKD-MBD): Back to Basics. Am J Kidney Dis. 2021; 78: 582-589

Piek, E. and Roberts, A. B. Suppressor and oncogenic roles of transforming growth factor-beta and its signaling pathways in tumorigenesis. Adv Cancer Res. 2001; 83: 1-54

Reid, I. R. and Billington, E. O. Drug therapy for osteoporosis in older adults. Lancet. 2022; 399: 1080-1092

Riggs, B. L., Khosla, S. and Melton, L. J., 3rd Sex steroids and the construction and conservation of the adult skeleton. Endocr Rev. 2002; 23: 279-302

Shane, E., Burr, D., Abrahamsen, B., Adler, R. A., Brown, T. D., Cheung, A. M., Cosman, F., Curtis, J. R., et al. Atypical subtrochanteric and diaphyseal femoral fractures: second report of a task force of the American Society for Bone and

Mineral Research. J Bone Miner Res. 2014; 29: 1-23

Singer, A., Exuzides, A., Spangler, L., O'Malley, C., Colby, C., Johnston, K., Agodoa, I., Baker, J., et al. Burden of illness for osteoporotic fractures compared with other serious diseases among postmenopausal women in the United States. Mayo Clin Proc. 2015; 90: 53-62

Souza, P. P. and Lerner, U. H. The role of cytokines in inflammatory bone loss. Immunol Invest. 2013; 42: 555-622

Tamata, A. T. and Mohammadnezhad, M. A systematic review study on the factors affecting shortage of nursing workforce in the hospitals. Nurs Open. 2023; 10: 1247-1257

Tas, A. C. and Bhaduri, S. B. Rapid coating of Ti6Al4V at room temperature with a calcium phosphate solution similar to 10× simulated body fluid. Journal of Materials Research. 2004; 19: 2742-2749

Udagawa, N., Koide, M., Nakamura, M., Nakamichi, Y., Yamashita, T., Uehara, S., Kobayashi, Y., Furuya, Y., et al. Osteoclast differentiation by RANKL and OPG signaling pathways. J Bone Miner Metab. 2021; 39: 19-26

Yan, X., Zhang, S., Jia, J., Yang, J., Song, Y. and Duan, H. Exosomal MiR-423-3p inhibits macrophage M2 polarization to suppress the malignant progression of cervical cancer. Pathol Res Pract. 2022; 235: 153882

Yang, J., Li, Q., Feng, Y. and Zeng, Y. Iron Deficiency and Iron Deficiency Anemia: Potential Risk Factors in Bone Loss. Int J Mol Sci. 2023; 24:

Zhu, M., Xu, M., Bertheloot, D., Brom, V. C., Sieberath, A., Salber, J., Welle, K.,

Burger, C., et al. Arcyriaflavin A Alleviates Osteoporosis by Suppressing RANKL-Induced Osteoclastogenesis. Int J Mol Sci. 2025; 26:

53

2. Publication

This dissertation is based on the following peer-reviewed publication:

Zhu M, Xu M, Bertheloot D, Brom V C, Sieberath A, Salber J, Welle K, Burger C, Wirtz D C, Wang S, Schildberg F A, Arcyriaflavin A Alleviates Osteoporosis by Suppressing RANKL-Induced Osteoclastogenesis. International Journal of Molecular Sciences. 2025, 26(5), 2141

https://doi.org/10.3390/ijms26052141

3. Declaration of Personal Contribution

In general, Univ.-Prof. Dr. rer. nat. Frank A. Schildberg and I determined the initial concept. We decided to screen potential osteoclast inhibitors from compounds influencing macrophage polarization. Together with Prof. Schildberg, we planned and developed the detailed experimental design for this project. With Prof. Schildberg's help, I evaluated the suitability of candidates from the initial screen and selected the research object.

For mouse cell culture, I provided the experimental protocols for osteoclast culture, and all the experiments mentioned in section 1.2.1 were performed by me. Additionally, Mr. Werner Masson taught me the biosafety procedures for cell culture and tissue extraction.

The development and optimization of the formulations of media mentioned in section 1.2.2 were performed by me, referencing the protocol from the Research Laboratory of the Department of Orthopedics and Trauma Surgery, Universitätsklinikum Bonn.

The inhibitor screening and phenotype assays in sections 1.2.3 and 1.2.4 were conducted by me, and the evaluation of the results was carried out by myself and Prof. Schildberg.

The advanced bonelike apatitic calcium phosphate coating plates used for the function assay (section 1.2.5) were based on the protocol by Tas and Bhaduri (doi: 10.1557/JMR.2004.0349) and were provided by Dr. Alexander Sieberath and Prof. Jochen Salber from Ruhr-Universität Bochum.

Regarding PCR in section 1.2.6, I performed all PCR operations and data analysis, while Mr. Masson provided technical support.

55

With the protocol and technical support provided by Dr. Damien Bertheloot, I conducted the Western blot mentioned in section 1.2.6. Certain instruments for Western blot were shared by the Laboratory of Immunopathophysiology, Universitätsklinikum Bonn (Director: Prof. Dr. rer. nat. Sven Wehner).

For human cell culture and phenotype analysis in 1.2.7, Mr. Werner Masson performed experiments and conducted data analysis together with me, according to the protocol provided by Dr. Victoria C. Brom.

The animal experiments in section 1.2.8 were conducted in collaboration with the Second Hospital of Shanxi Medical University (Taiyuan, Shanxi, China). The animal experimental plan was jointly designed by myself, Prof. Schildberg, and Prof. Shaowei Wang (Shanxi Medical University) and carried out by Mr. Mingwei Xu from the Second Hospital of Shanxi Medical University. Data analysis for animal experiments was performed by me. In addition, all animal experiments were performed with the approval of the Ethics Committee of the Second Hospital of Shanxi Medical University (approval No. DW2023028).

The primary drafting of the manuscript—including the creation of figures, schematic diagrams, and tables—and the verification of statistical reliability were independently completed. Prof. Schildberg, Prof. Dr. med. Dieter C. Wirtz, Prof. Dr. med. Christof Burger, and PD Kristian Welle offered constructive feedback and assisted in refining the manuscript content.

I certify that I have written this dissertation independently and have not used any sources or resources other than those indicated. With the exception of the cases specifically noted above, most of the experimental work was conducted at the Research Laboratory of the Department of Orthopedics and Trauma Surgery, Universitätsklinikum Bonn.

4. Acknowledgement

First and foremost, I would like to express my sincere gratitude to my supervisor, Prof. Frank A. Schildberg, for entrusting me with this meaningful research project and for providing invaluable support and guidance. throughout the course of my experiments, I encountered numerous challenges and setbacks, but Prof. Schildberg always encouraged me and engaged in discussions to approach solutions.

I am especially grateful to our experienced technician Mr. Werner Masson, who provided me with tremendous assistance and guidance in experimental procedures. His meticulous management keeps the laboratory well-organized, the working environment excellent. Additionally, I deeply appreciate Werner's help with the culture and counting of human osteoclasts.

Furthermore, I would like to extend my gratitude to Prof. Shaowei Wang and Mr. Mingwei Xu from Shanxi Medical University for their assistance in the animal experiments. Dr. Damien Bertheloot helped me refine the Western blot technique, and Prof. Jochen Salber and Dr. Alexander Sieberath from Bochum provided exceptionally effective culture plates that greatly benefited this research. Moreover, thanks to the laboratory of Immunpathophysiology (Director: Prof. Dr. rer. nat. Sven Wehner) for sharing devices and equipment.

The achievements of this study are undoubtedly the result of our teamwork. Every piece of data obtained, whether included in this paper or not, has contributed to the rigority of this work. I sincerely thank every member of the laboratory, including those mentioned above, as well as Dr. El-Mustapha Haddouti, Dr. Robert Ossendorf, and Dr. Jayagopi Surendar, for making the lab feel like a warm family, giving me a sense of belonging.

57

I also wish to thank the staff at the Promotionsbüro for their support and guidance during my time at the university. A special thanks to Mr.

Patrick.Schleicher, our former lab secretary. Although he has left the position, I remain deeply grateful for his help when I first arrived, from assisting me in finding an amazing apartment to handling various administrative procedures.

During my time in UKB, I have attended several insightful conferences. Hence, I would like to extend my appreciation to UKB and Prof Dieter C. Wirtz and Prof. Christof Burger for making these opportunities possible. Lastly, I am immensely grateful for the unwavering support and encouragement from my family and friends.

Time has flown by—the oak tree outside the lab window has cycled from budding to full bloom, from golden leaves to being blanketed in snow. Now, for the fourth time, I witness its fresh leaves is emerging. I can already picture the magnolias blooming in the Botanische Gärten in the Poppelsdorfer Schloss. So, one final thank-you goes to Bonn—a beautiful city that has given me an unforgettable experience.